This is an open access article published under a Creative Commons Non-Commercial No Derivative Works (CC-BY-NC-ND) Attribution License, which permits copying and redistribution of the article, and creation of adaptations, all for non-commercial purposes.

ACS AUTHORCHOICE

Journal of Medicinal Chemistry

Article

Cite This: J. Med. Chem. 2020, 63, 241−259

pubs.acs.org/jmc

Ligand-Based Design of Allosteric Retinoic Acid Receptor-Related Orphan Receptor γt (RORγt) Inverse Agonists

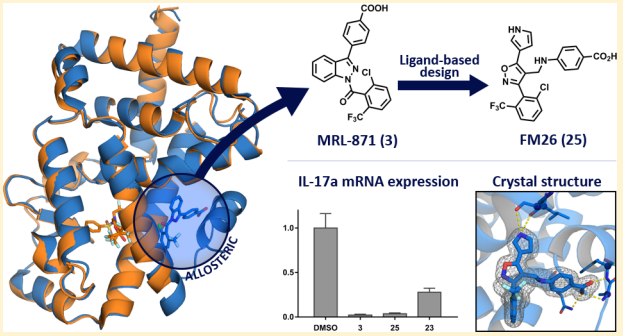
Femke A. Meijer,[ξ,†] Richard G. Doveston,[ξ,†,‡] Rens M.J.M. de Vries,[†] Gaël M. Vos,[†] Alex A.A. Vos,[†] Seppe Leysen,[†] Marcel Scheepstra,[†] Christian Ottmann,[†] Lech-Gustav Milroy,[†] and Luc Brunsveld*[,†]

[†]Laboratory of Chemical Biology, Department of Biomedical Engineering and Institute for Complex Molecular Systems, Technische Universiteit Eindhoven, Den Dolech 2, 5612 AZ Eindhoven, The Netherlands

[‡]Leicester Institute of Structural and Chemical Biology and Department of Chemistry, University of Leicester, University Road, Leicester LE1 7RH, U.K.

Supporting Information

ABSTRACT: Retinoic acid receptor-related orphan receptor γt (RORγt) is a nuclear receptor associated with the pathogenesis of autoimmune diseases. Allosteric inhibition of RORγt is conceptually new, unique for this specific nuclear receptor, and offers advantages over traditional orthosteric inhibition. Here, we report a highly efficient in silico-guided approach that led to the discovery of novel allosteric RORγt inverse agonists with a distinct isoxazole chemotype. The the most potent compound, **25** (**FM26**), displayed submicromolar inhibition in a coactivator recruitment assay and effectively reduced IL-17a mRNA production in EL4 cells, a marker of RORγt activity. The projected allosteric mode of action of **25** was confirmed by biochemical experiments and cocrystallization with the RORγt ligand binding domain. The isoxazole compounds have promising pharmacokinetic properties comparable to other allosteric ligands but with a more diverse chemotype. The efficient ligand-based design approach adopted demonstrates its versatility in generating chemical diversity for allosteric targeting of RORγt.



1. INTRODUCTION

The nuclear receptor (NR) RORγt has emerged as an important therapeutic target in recent years because of its important role in both cancer and autoimmune disease. Inhibition of RORγt is a promising therapeutic strategy for the treatment of prostate cancer because it stimulates androgen receptor (AR) gene transcription.[1,2] However, RORγt is most prominently targeted for inhibition because of its essential role in promoting T helper 17 (Th17) cell differentiation.[3−5] Th17 cells produce the cytokine IL-17 which is strongly implicated in the pathogenesis of autoimmune diseases[6] such as psoriasis,[7] multiple sclerosis,[8] and inflammatory bowel disease.[9] Disrupting the Th17/IL-17 pathway using IL-17 monoclonal antibodies (mAb) is a successful therapeutic strategy, with three mAbs approved for the treatment of plaque psoriasis: secukinumab (Cosentyx),[10] brodalumab (Siliq),[11] and ixekizumab (Taltz).[12] Inhibition of RORγt with small molecules to disrupt the Th17/IL-17 pathway has been the focus of much research in recent years,[13−20] with several compounds having progressed to clinical trials.[2]

RORγt contains a hydrophobic ligand binding pocket located within a ligand binding domain (LBD) that is highly conserved across the NR family.[21] However, its transcriptional activity is not dependent on ligand binding because the apo protein retains the C-terminal helix 12 (H12) in a conformational state that allows for partial recruitment of coactivator proteins.[22,23] Although formally an orphan receptor with no proven endogenous ligands, RORγt is responsive to binding of naturally occurring cholesterol derivatives. Hydroxycholesterols have been shown to be effective agonists that stabilize H12 in such a way to further promote coactivator binding.[24] In contrast, digoxin (**1**, Figure 1) is an inverse agonist that stabilizes H12 in a conformation that is unsuitable for coactivator binding but promotes corepressor binding, thus leading to diminished gene transcription.[25] Numerous synthetic inverse agonists are also known, including T0901317 (**2**, Figure 1).[26] In all these cases, the ligands target the same orthosteric ligand binding pocket (Figure 1).

NR orthosteric ligand binding pockets are the target for numerous and highly effective drug molecules.[27] Nevertheless, the highly conserved nature of this pocket across the NR family has led to issues associated with selectivity and mutation-induced resistance. Furthermore, dosing levels must be appropriate to compete with endogenous ligands. Molecules that target allosteric binding sites on NRs could circumvent such problems, for example because of the chemical uniqueness of the pocket and the absence of a competitive

Received: August 20, 2019
Published: December 10, 2019

Downloaded via UNIV OF LEICESTER on February 5, 2020 at 15:53:33 (UTC).
See https://pubs.acs.org/sharingguidelines for options on how to legitimately share published articles.

© 2019 American Chemical Society

DOI: 10.1021/acs.jmedchem.9b01372
J. Med. Chem. 2020, 63, 241−259

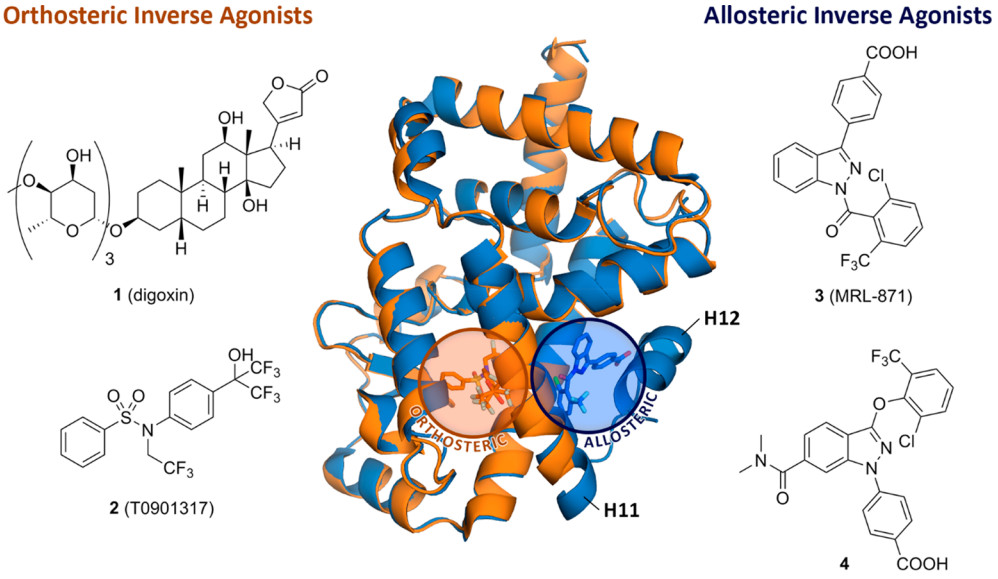


Figure 1. Orthosteric and allosteric RORγt ligand binding sites are shown by overlay of the crystal structures of RORγt LBD in complex with orthosteric inverse agonist **2** (orange, PDB code: 4NB6) and allosteric inverse agonist **3** (blue, PDB code: 4YPQ). The structures of the orthosteric inverse agonist **1** and allosteric inverse agonist **4** are also shown.

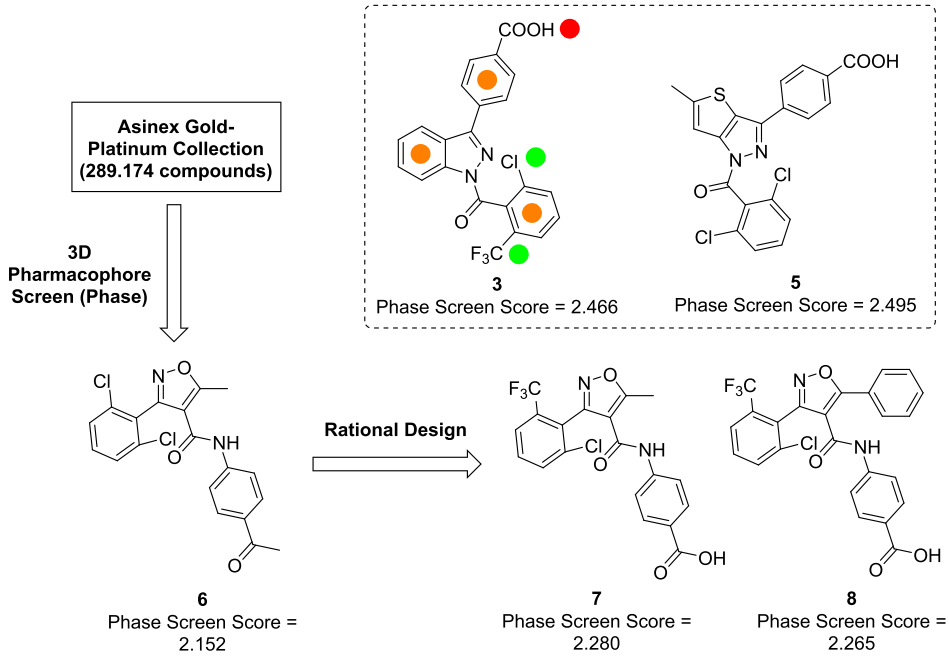


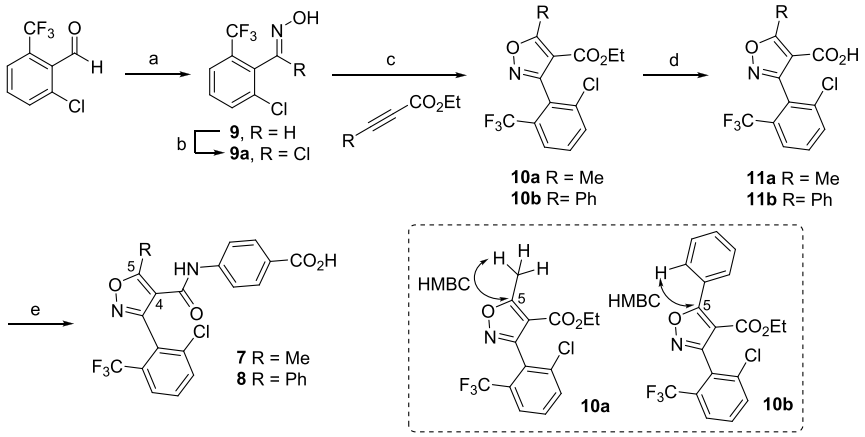
Figure 2. 3D Pharmacophore screening identifies a compound class with a novel isoxazole-based chemotype for experimental evaluation. The structural features of **3** incorporated into the pharmacophore hypothesis are indicated: orange = aromatic rings, green = hydrophobic groups, and red = anionic group.

endogenous ligand. Such allosteric compounds are therefore extremely valuable for both drug discovery and chemical biology applications.[28−30] The discovery that the potent RORγt inverse agonists MRL-871 (**3**, Figure 1)[31] and later **4**[32] target a previously unreported allosteric binding site within the RORγt LBD was therefore highly significant. These ligands were observed to directly interact with the activation function loop between H11 and H12 (AF-2 domain), thus forcing H12 to adopt an unusual conformation that prevents coactivator recruitment (Figure 1).[31]

Allosteric modulation of RORγt has enormous potential as a novel therapeutic strategy, but the examples of ligands that unambiguously target the allosteric pocket have been limited to compounds based on closely related chemotypes containing indazole or imidazopyridine cores.[28] As an example, indazoles **3** and **4** displayed promising in vivo activity,[33,34] but challenges remain, such as PPARγ cross-activity and pharmacokinetic (PK) profiles, for which novel chemotypes are needed.[15] In order to better exploit the strategy of allosteric modulation for therapeutic purposes, there is thus an urgent need to identify novel chemotypes targeting the allosteric site. In this study, we report the design, synthesis, and evaluation of a novel class of RORγt allosteric inverse agonists. The novel chemotype, discovered by in silico-guided pharmacophore screening and

DOI: 10.1021/acs.jmedchem.9b01372
J. Med. Chem. 2020, 63, 241−259

Scheme 1. Synthesis of Trisubstituted Isoxazoles 7 and 8[a]



[a]Key HMBC correlations used to confirm the regiochemistry of **10a** and **10b** are shown. The ^{13}C-NMR signals for the C-5 carbons are distinctively downfield at 175 and 173 ppm, respectively. Reagents and conditions: (a) $NH_2OH{\cdot}HCl$, NaOH (aq), EtOH, rt, 18 h, 83%; (b) NCS, DMF, 60 °C, 18 h, 86%; then (c) alkyne, NEt_3, THF, 80 °C, 4 h, 69% (**10a**), 80% (**10b**); (d) LiOH, EtOH, H_2O, 70 °C, 8 h, 84% (**11a**), 95% (**11b**); and (e) (i) $SOCl_2$, 50 °C, 2 h; (ii) *tert*-butyl-4-amino benzoate, NEt_3, CH_2Cl_2, 45 °C, 6 h; and (iii) TFA, CH_2Cl_2, rt, 18 h, 42% (**7**), 69% (**8**).

optimization, is based on a trisubstituted isoxazole core that, following efficient optimization of two substituents, led to the discovery of a submicromolar inverse agonist. Protein X-ray crystallography and biophysical data unambiguously proved the designed allosteric mode of action. The compounds effectively inhibit cellular IL-17a expression and thus constitute valuable leads in the development of treatments for autoimmune diseases. To the best of our knowledge, our highly efficient in silico-guided approach is the first example of a medicinal chemistry program to overtly identify and develop a novel chemotype that targets the RORγt allosteric site.

2. RESULTS AND DISCUSSION

2.1. In Silico Pharmacophore Screen. In order to identify novel chemotypes for chemical optimization, we used the crystal structure of RORγt LBD in complex with **3** as the basis for an in silico 3D pharmacophore screen against virtual compound libraries. An analogous scaffold hopping approach had been used previously to identify similar scaffolds to **3** such as the potent inverse agonist thienopyrrazole **5** (Figure 2), although an allosteric mode of action was not proven.[35] We created a 3D pharmacophore hypothesis based on the crystal structure of **3** bound to the allosteric pocket using Phase (Schrödinger 2017−2).[36,37] Six structural features of **3** known to be important for activity were incorporated in the hypothesis: the three six-membered aromatic rings, an anionic group, and two hydrophobic substituents (Figure 2). This hypothesis was used to interrogate a virtual library of 289,174 compounds from the Asinex Gold−Platinum collection of drug-like molecules.[38] Compounds matching at least four out of the six pharmacophore features were deemed to be a good hit. These were ranked using the "Phase Screen Score" with higher scores indicating a better alignment with the hypothesis. The Phase Screen scores for **3** and **5** were used as contextual references. The four highest ranking hit structures were all found to be based around the same trisubstituted isoxazole scaffold with **6** returned as the best match (Figure 2). This same scaffold was present in 13 of the top 30 hits. However, in each case we noted that only four out of six pharmacophore features were matched. Therefore, we designed two virtual ligands, **7** and **8**, that incorporated five and six of the features, respectively. As expected, this led to improved Phase Screen Scores (Figure 2), and these compounds were therefore selected as initial targets for experimental investigation.

2.2. Exploratory Structure−Activity Relationship Study. Isoxazoles **7** and **8** were synthesized via [3 + 2] dipolar cycloaddition of a nitrile oxide (generated in situ from the oxime chloride **9a**) and a commercially available alkyne.[39] The regiochemistry of the resulting trisubstituted isoxazole esters **10** was confirmed by 2D-NMR experiments (key HMBC correlations are highlighted in Scheme 1). Ester hydrolysis followed by amide coupling of *tert*-butyl-4-amino benzoate via the respective acid chloride, and finally deprotection of the *tert*-butyl ester furnished the target compounds in an efficient manner (Scheme 1).

To determine if the compounds showed a functional response in terms of RORγt affinity for a coactivator, **7** and **8** were tested in a time-resolved FRET (TR-FRET) coactivator recruitment assay.[31] Remarkably, both compounds inhibited coactivator recruitment in a dose-dependent manner. The phenyl derivative **8** was found to be significantly more potent than the methyl derivative **7**: half-maximum inhibitory concentrations (IC_{50}) of 53.5 ± 2.9 μM for **8** compared to >100 μM for **7**. In line with previous reports, **3** and **5** were determined to be significantly more potent with an IC_{50} of 7.8 ± 0.5 nM and 425 ± 61 nM, respectively (Table 1).

In view of these highly promising TR-FRET results with the in silico derived compounds around the trisubstituted isoxazole scaffold already showing activity, phenyl isoxazole **8** was selected as the focus of a subsequent structure−activity relationship (SAR) study focusing on the isoxazole C-4 position. As such, a small library of 11 derivatives was synthesized using carboxylic acid **11b** as the cornerstone intermediate (Scheme 2) and evaluated using the coactivator recruitment assay (Table 1). While limited in size, this SAR study indicated that a benzoic acid-containing substituent at the C-4 position was essential for potency: examples bearing no C-4 substitution (**11b**), a *para*-benzoate (**14**), or a methylene carboxylic acid (**15**) showed much reduced potency compared to the initial hit. Moving the acid moiety to the meta-position (**16**) or adding a *meta*-fluoro substituent (**17**) somewhat lowered the activity. However, the insertion of a

DOI: 10.1021/acs.jmedchem.9b01372
J. Med. Chem. 2020, 63, 241−259

Table 1. Structure-Activity Relationships around the C-4 Isoxazole Position[a]

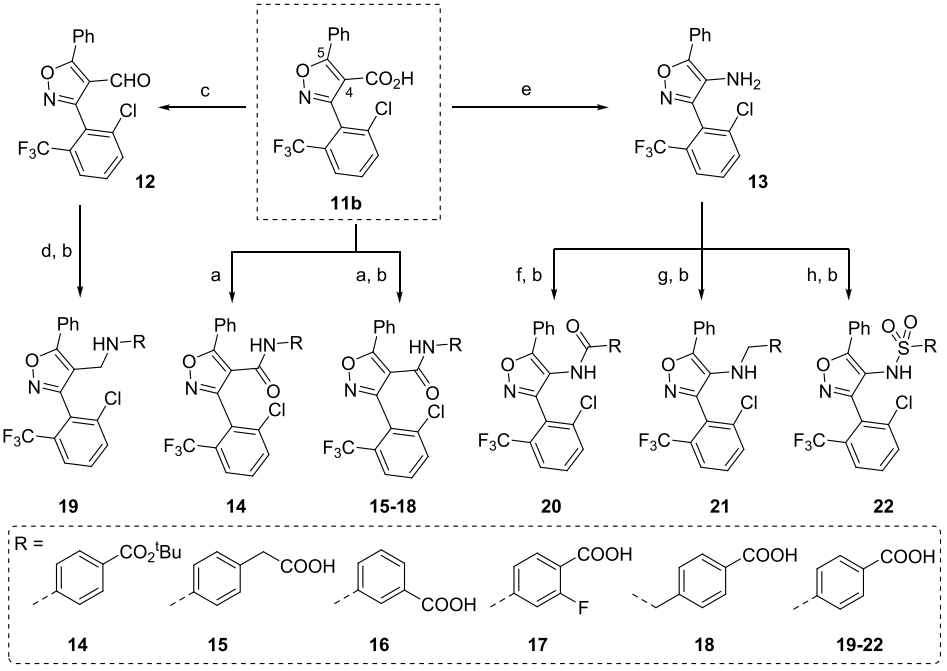
cmpd	IC_{50} (μM)	Glide score
3	0.0078 ± 0.0005	− 14.576
5	0.425 ± 0.061	− 13.109
7	>100	− 13.372
8	53.5 ± 2.9	− 14.184
11b	>100	− 10.130
14	>100	n.d.
15	>100	− 13.724
16	73.9 ± 3.4	− 12.995
17	91.1 ± 4.6	− 14.308
18	8.76 ± 0.48	− 12.020
19	9.60 ± 0.60	− 14.012
20	>100	− 13.550
21	30.9 ± 1.3	− 13.519
22	62.6 ± 4.4	− 13.003

[a]TR-FRET IC_{50} values (μM) and respective Glide docking scores are shown. TR-FRET data is recorded in triplicate; values are representative of >3 repeated experiments.

single methylene unit between the amide and benzoic acid moieties (**18**) led to a 6-fold increase in potency compared to the initial hit. The corresponding amine (**19**) displayed similar activity. Finally, reversing the relative positions of carbonyl and nitrogen components of the amide bond (**20**−**22**) did not result in a corresponding increase in potency.

2.3. In Silico Docking Directs Secondary SAR Study. In order to further improve the potency of our compounds, we next explored the SAR at the isoxazole C-5 position. For this, molecular docking (Glide, Schrodinger 2017−2)[40,41] was used to select, with an attention to synthetic resource, C-5 substituents that were optimal for allosteric binding and therefore activity. For the study, a single C-4 substituent, the amine of compound **19** was chosen based on its experimental activity and in silico docking score (Table 1, vide infra). A virtual library of 84 C-5 analogues was enumerated using the open-source ChemT software.[42] This library was docked against the allosteric site of RORγt as defined by the X-ray crystal structure of **3** in complex with the RORγt LBD.[31] A single docking pose was returned for each virtual ligand, and these were ranked using the "Glide Score", an empirical measure of binding enthalpy.[43] We contextualized these scores by comparison to those of compounds with known activity. The results (summarized in Table 2, see Supporting Information for full information) indicated that smaller heteroaromatic moieties at the C-5 position would improve allosteric binding of the isoxazole ligands relative to **19**, heteroatoms at the 2-postion were predicted to be optimal, for example, furan **23** and thiophene **24** (Table 2). The introduction of a hydrogen-bond donor on the ring (specifically at the 3-position) was predicted to be even more beneficial: docking poses indicated that an additional hydrogen-bonding interaction with the backbone of helix 4 might be possible (e.g., pyrrole **25**, Table 2, Figure 3). Bulkier substituents were predicted to be detrimental for binding (e.g., naphthyl **26**). To explore the predicted effect of a hydrogen-bond donating group further we interrogated a designed subset of ligands in the same docking experiment (see the Supporting Information). None of these ligands showed an improved Glide score compared to pyrrole **25**. However, we noted that 3-hydroxyl substitution of the C-5 phenyl ring (**27**) was predicted to significantly enhance binding relative to **19**. To

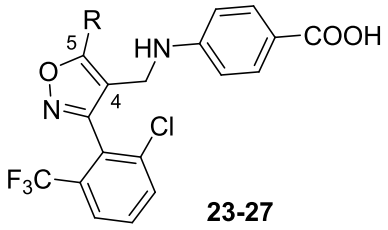
Scheme 2. Synthesis of C-4 Isoxazole Derivatives[a]



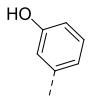
[a]Reagents and conditions: (a) (i) $SOCl_2$, 50 °C, 2 h; (ii) NH_2R, NEt_3, CH_2Cl_2, 45 °C, 6 h, 27−87%; (b) LiOH, MeOH, H_2O, 70 °C, 8 h, 43−99%; (c) (i) $SOCl_2$, 50 °C, 2 h; (ii) MeNH(OMe), NEt_3, CH_2Cl_2, rt, 6 h; (iii) $LiAlH_4$, THF, 0 °C, 30 min, 65%; (d) (i) ethyl-4-aminobenzoate, AcOH, MeOH, reflux, 24 h; (ii) $NaCNBH_3$, MeOH, reflux, 12 h, 31%; (e) (i) DPPA, *t*-BuOH, 85 °C, 18 h; (ii) TFA, CH_2Cl_2, rt, 8 h, 59%; (f) (i) monomethyl terephthalate, $SOCl_2$, 50 °C, 2 h; (ii) **13**, NEt_3, CH_2Cl_2, 76%; (g) (i) methyl-4-formyl benzoate, AcOH, MeOH, reflux, 24 h; (ii) $NaCNBH_3$, MeOH, reflux, 18 h, 43%; and (h) methyl-4-(chlorosulfonyl)benzoate, pyridine, 60 °C, 24 h, 71%.

DOI: 10.1021/acs.jmedchem.9b01372
J. Med. Chem. 2020, 63, 241−259

Table 2. Structure-Activity Relationships around the C-5 Isoxazole Position[a]



23-27

Cmpd	R	Glide Score	IC_{50} (μM)
19	Ph	– 14.012	9.60 ± 0.60
23		– 14.300	1.09 ± 0.09
24		– 14.182	1.75 ± 0.20
25		– 15.735	0.264 ± 0.023
26		– 10.844	> 100
27		– 14.603	6.62 ± 0.50

[a]TR-FRET IC_{50} values (μM) and respective Glide docking scores are shown. TR-FRET data is recorded in triplicate; values are representative of >3 repeated experiments.

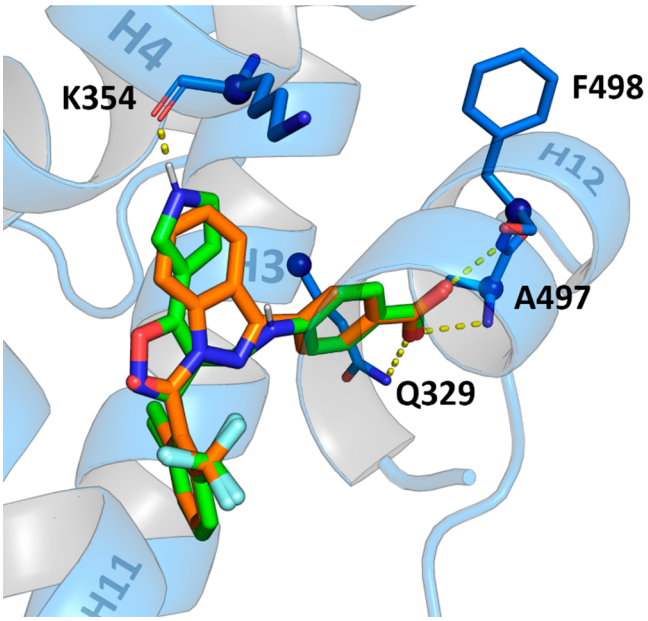
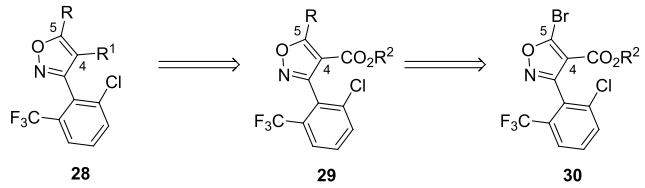


Figure 3. In silico modeled docking pose of **25** (green) overlaid with crystal structure of RORγt with **3** (orange) (PDB code: 4YPQ). For **25**, the potential additional hydrogen bond with the RORγt H4 backbone is indicated.

validate our findings experimentally, we selected a cross section of five derivatives for synthesis (i.e., **23**–**27**).

2.4. Docking-Guided C-5 SAR Study. To expedite the synthesis of isoxazole analogues with various C-5 and C-4 substituents, we redesigned our synthetic approach. It was envisaged that 5-bromo-4-carboxy isoxazole intermediate **30** would enable later stage introduction of the desired C-5 substituents via palladium-mediated cross-coupling chemistry. Introduction of C-4 substituents by manipulation of a carbonyl functional group (as developed previously) would then be possible (Scheme 3).

Scheme 3. Retrosynthetic Analysis of Trisubstituted Isoxazole 28 Allowing for Late-Stage Diversification



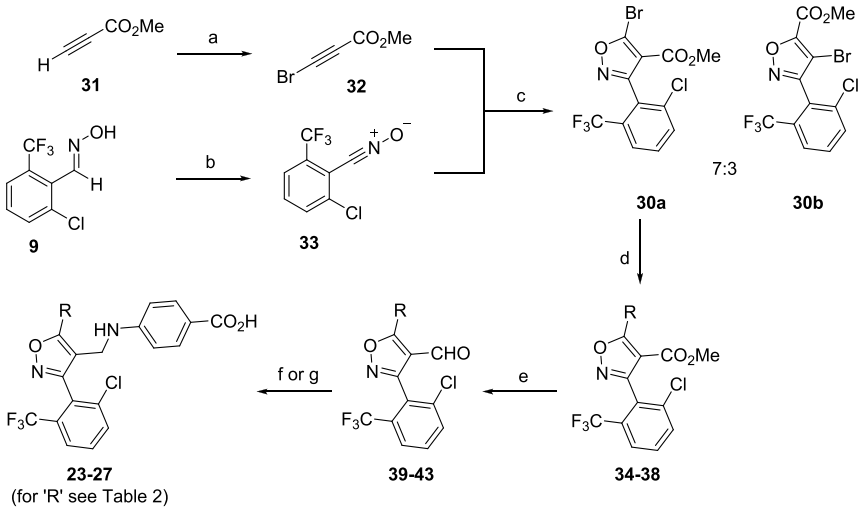
The intermediate **30** was prepared using analogous methodology to that used previously. In this case it was necessary to isolate nitrile oxide **33** prior to [3 + 2] cycloaddition with alkynyl bromide **32**.[44] An efficient cycloaddition reaction led to an essentially quantitative recovery of a 7:3 mixture of 5-bromoisoxazole **30a** and 4-bromoisoxazole **30b** as determined by ^{1}H NMR (Scheme 4). This result was in close alignment with literature examples that indicated the 5-bromo isomer would predominate.[44] The mixture of regioisomers was purified by recrystallization from hot *n*-heptane resulting in the isolation of a 97:3 regiomeric mixture (43% recovery) that was employed in subsequent steps. Assignment of the 5-bromoisoxazole **30a** as the major regioisomer was confirmed by 2D-NMR analysis of downstream products and by synthesis via an independent route (see the Supporting Information).

The desired substituents were introduced at the C-5 position by way of a Suzuki cross-coupling with a pinacol boronate[45] (to give intermediates **34**–**38**) before conversion of the C-4 ester to an aldehyde (**39**–**43**) and reductive amination (Scheme 4). The lability of the 5-bromo group under the conditions for ester reduction dictated the order in which the synthesis steps were performed. Hydrolysis of the benzoic methyl ester to the free acid yielded the desired compounds **23**–**27**.

In order to explore the SAR around the isoxazole C-5 position, the five analogues prepared in this second synthesis campaign were evaluated using the HTRF coactivator recruitment assay (Table 2). We were gratified to observe that furan **23** gave a 9-fold improvement in potency compared to phenyl **19**. By comparison, thiophene **24** was slightly less potent. Most significantly, pyrrole **25**, which also showed the most beneficial Glide score, was 36-fold more potent than **19** and with an IC_{50} value lower than the putative allosteric modulator **5**. These results were in excellent agreement with the in silico Glide scores obtained (Table 2), and the improvements in potency are a notable step toward emulating the high potency of indazole **3** (Figure 4A). As predicted, the bulky naphthyl group of **26** was detrimental for activity such that no IC_{50} curve could be fitted. The phenol derivative **27** showed a small improvement in potency compared to **19**. For

DOI: 10.1021/acs.jmedchem.9b01372
J. Med. Chem. 2020, 63, 241–259

Scheme 4. Synthesis of Isoxazole C-5 Analogues 23−27.[a]



[a]"R" groups are defined in Table 2. Reagents and conditions: (a) NBS, $AgNO_3$, $Me_2C(O)$, rt, 20 h, 80%; (b) (i) NCS, DMF, 60 °C, 18 h, (ii) NEt_3, THF, rt, 30 min, 85%; (c) THF, 80 °C, 4 h, **30a** 43%; (d) RB(pin), $Pd(dppf)Cl_2$, DME, 85 °C, 8 h, 39−58%; (e) (i) $LiAlH_4$, THF, 0 °C → rt, 2 h, then (ii) DMP, CH_2Cl_2, rt, 8 h, 51−96%; (f) *tert*-butyl-4-amino benzoate, MeOH, AcOH, reflux, 24 h then (ii) $NaBH_4$, EtOH, 85 °C, 2−6 h, 16−24%; (iii) TFA, CH_2Cl_2, rt, 18 h, **23**, **24**, **26**, 48−73%; and (g) methyl-4-amino benzoate, MeOH, AcOH, reflux, 24 h then (ii) $NaBH_4$, MeOH, reflux, 2−4 h, 16−19%; and (iii) LiOH, MeOH, H_2O, 70 °C, 8 h, **25**, 57%, **27**, 99%.

this more bulky group at the C-5 position, compared to pyrrole **25**, the potential for additional hydrogen bonding, as indicated in the docking study, is thus not strongly expressed.

2.5. Mode-of-Action Studies. The allosteric mode-of-action for the novel lead compound **25** was first explored using a competitive TR-FRET coactivator recruitment assay against fixed concentrations of cholesterol (an orthosteric agonist). If an allosteric ligand and cholesterol bind in a noncompetitive manner at different sites on the RORγt LBD then the IC_{50} of the allosteric ligand should be independent of cholesterol concentration. By contrast, ligands competing for the same binding site should show a cholesterol-dependent activity profile whereby increasing cholesterol concentration should result in a corresponding increase in IC_{50} of the competing ligand.[31] In our assay, increasing concentrations of **25** perturbed coactivator recruitment in the absence of cholesterol with an IC_{50} value of 247.8 ± 17.7 nM. Interestingly, increasing concentrations of cholesterol indeed resulted not in an increase but in a further decrease in the IC_{50} value for **25** with a concomitant sharpening of the Hill slope (Figure 4B and Table 3). This result provides strong evidence not only for an allosteric mode-of-action but also for cooperative behavior between orthosteric and allosteric ligand binding. The same profile was observed for **5** (Figure 4C), providing the first evidence that this compound also modulates RORγt activity in an allosteric fashion. Indazole **3** also exhibited this behavior (Figure 4D). By comparison, the IC_{50} value for the orthosteric inverse agonist **1** increased as the concentration of cholesterol increased (Figure 4E). Collectively, our competitive assay data provided strong evidence that **25** functioned as an allosteric inverse agonist.

To further confirm the allosteric mode-of-action for **25** on RORγt, we used an orthogonal assay to directly probe for allosteric ligand binding, as opposed to measuring indirect effects on coactivator recruitment. This assay used the previously described AlexaFluor647-labeled MRL-871 derivative **44** (Figure 4G), which upon binding to RORγt shows fluorescent emission as a result of FRET from an anti-His terbium cryptate antibody donor.[32] The results of this experiment indeed corroborated the data obtained from the competitive cofactor recruitment assay (Figure 4F): the isoxazole **25** displaced the allosteric probe **44** with an IC_{50} = 117.5 ± 8.5 nM, which was lower than that of **5** (IC_{50} = 180.0 ± 17.5 nM). As expected, indazole **3** was highly potent (IC_{50} = 17.3 ± 1.4 nM).

Indazole **3** had previously been shown to be selective for RORγt over other NRs (>100-fold), with only minor cross-activity on PPARγ.[31] To give an indication of the cross-reactivity of the isoxazole series on PPARγ, an HTRF coactivator recruitment assay was performed with compounds **3**, **5**, and isoxazoles **19** and **23**−**27**. **3** and **5** show IC_{50} values of 7.2 μM and 14.7 μM, respectively, for PPARγ (vs 7.8 nM and 425 nM for RORγt) (Table 4), meaning that they show some cross-reactivity to PPARγ but still are 923- and 35-fold selective for RORγt. **25** and all other compounds of the isoxazole series result in only weak to no PPARγ inhibition (IC_{50} values >50 μM), indicating that the isoxazole scaffold leads to favorably low PPARγ cross-reactivity. Thus, these data indicate that the novel class of allosteric isoxazole inverse agonists features potential as efficacious and selective RORγt inverse agonists.

2.6. Crystallography. Co-crystallization studies were performed for the most potent isoxazole **25** with the RORγt-LBD, to provide molecular insights in the ligand−receptor interaction. Crystals grew in a $P6_122$ space group and diffracted to a resolution of 1.61 Å (Table S6). In the experimental electron density map, clear density for compound **25** is observed in the allosteric site, formed by helices 4, 5, 11, and 12 (Figure 5A, Figure S2). The compound binds to this allosteric site in a similar orientation as **3** (Figure 5B), as was predicted by our docking studies (Figure 3). The 2,6-disubstituted phenyl ring common to both **3** and of **25** is located in the exact same part of the binding pocket (Figure 5B). Moreover, hydrogen-bonding interactions between the

DOI: 10.1021/acs.jmedchem.9b01372
J. Med. Chem. 2020, 63, 241−259

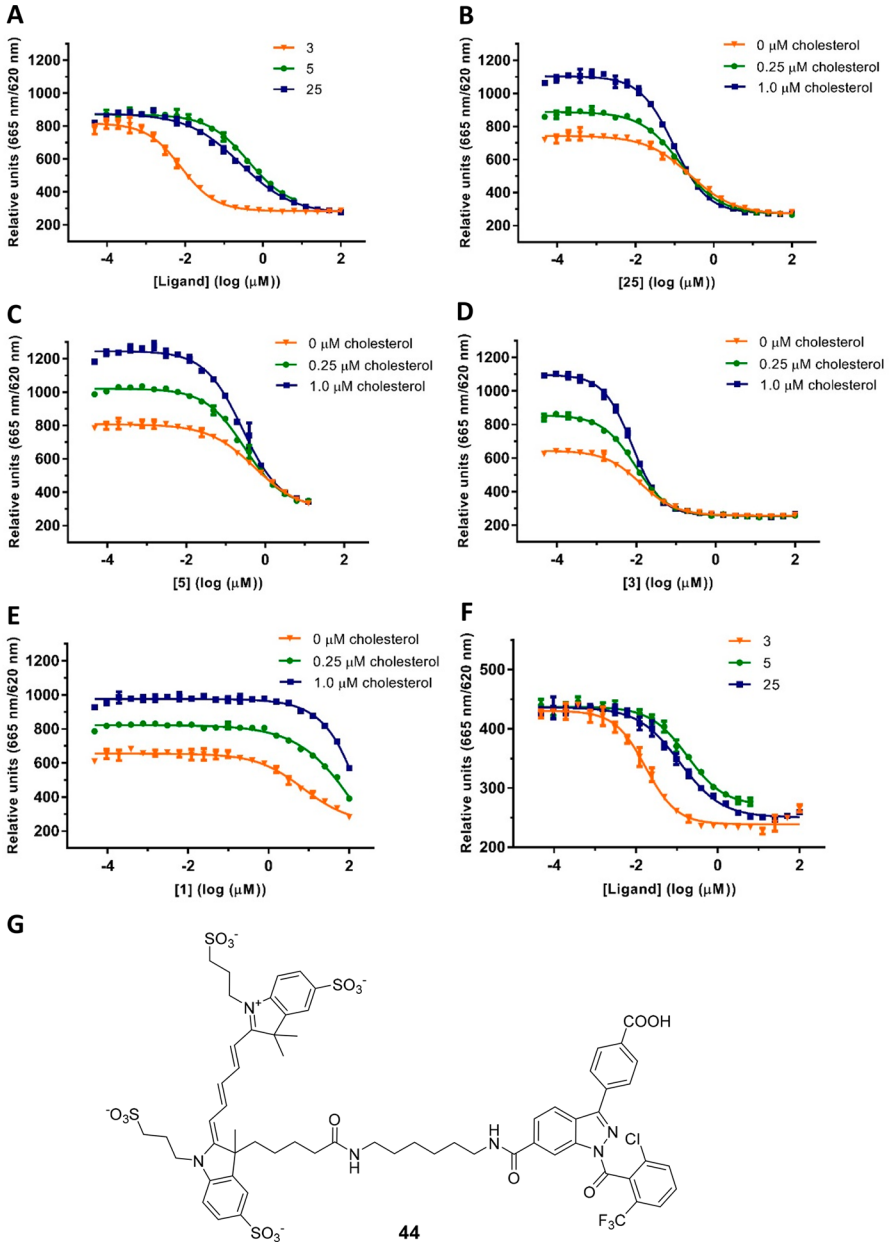


Figure 4. Biochemical RORγt assay data for **25**, **3**, and **5**. (A) Dose−response curves from the TR-FRET coactivator recruitment assay; (B−E) dose−response curves from the competitive TR-FRET coactivator recruitment assay with fixed concentrations of cholesterol (0, 0.25, and 1.0 μM); and (F) dose−response curves from the ligand displacement HTRF assay using **44** (G) as an allosteric probe.

Table 3. IC_{50} and Hill Slope Values Observed in the Competitive TR-FRET Cofactor Recruitment Assay

	0 μM cholesterol		0.25 μM cholesterol		1.0 μM cholesterol	
compound	IC_{50} (nM)	Hill slope	IC_{50} (nM)	Hill slope	IC_{50} (nM)	Hill slope
25	247.8 ± 17.7	−0.77 ± 0.04	138.0 ± 5.9	−0.86 ± 0.03	94.1 ± 3.3	−1.01 ± 0.03
5	547.3 ± 60.1	−0.74 ± 0.06	299.5 ± 18.0	−0.87 ± 0.04	268.9 ± 18.8	−0.90 ± 0.05
3	12.7 ± 0.6	−0.97 ± 0.04	9.4 ± 0.3	−1.04 ± 0.03	7.8 ± 0.2	−1.20 ± 0.03
1	7012 ± 588	−0.76 ± 0.05	33620 ± 1649	−0.77 ± 0.03	85400 ± 4276	−1.01 ± 0.06

carboxylic acid group and the main-chain amide hydrogen atoms of A497 and F498, as well as with the side chain of residue Q329, are also evident in both structures. Unique to **25** is the pyrrole ring, which is oriented to allow a hydrogen bond interaction with the main-chain carbonyls of residues L353 and K354 (Figure 5C). The isoxazole scaffold also allows a deeper penetration of this compound toward helix 4 of RORγt. In the case of isoxazole **25**, the AF-2 loop of the protein and the allosteric ligand are positioned slightly further apart as compared to **3** (Figure 5B). These structural data provide clear evidence for the allosteric binding of **25** to RORγt in an orientation that was predicted with remarkable accuracy in the docking study (Figure S3) but with specific additional

DOI: 10.1021/acs.jmedchem.9b01372
J. Med. Chem. 2020, 63, 241−259

Table 4. IC_{50} Values Observed in the Competitive TR-FRET Cofactor Recruitment Assay with PPARγ

compound	IC_{50} (μM)
3	7.2 ± 0.8
5	14.7 ± 1.0
19	78.6 ± 5.6
23	>100
24	>100
25	99.3 ± 6.4
26	>100
27	>100

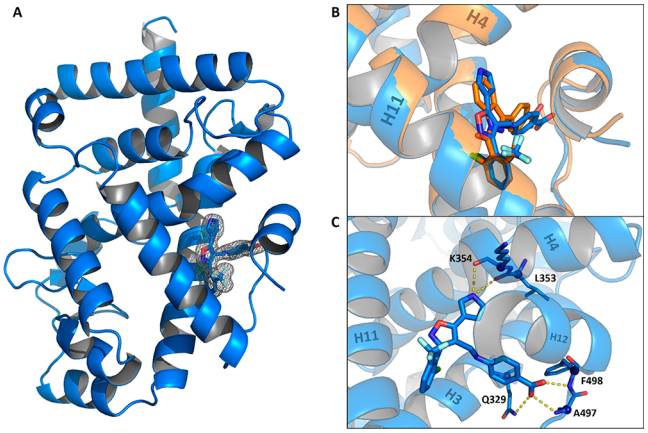


Figure 5. Co-crystal structure of RORγt with compound **25** (PDB code: 6SAL). (A) The tertiary structure of RORγt bound to **25** (stick representation). The final 2Fo−Fc electron density map of **25** is shown as an isomesh contoured at 1σ; (B) overlay of the crystal structure of RORγt bound to **25** and RORγt bound to **3** (PDB code: 5C4O); and (C) zoom-in on the allosteric pocket of RORγt showing the interactions between **25** and the protein.

molecular effects resulting from the novel isoxazole scaffold and pyrrole based substition pattern.

2.7. Isoxazole 25 Inhibits IL-17a Expression in EL4 Cells. EL4 is a murine lymphoblast cell line that constitutively expresses RORγt. Because RORγt promotes IL-17a production, an effective means to determine the cellular activity of RORγt inverse agonists is to measure the reduction in IL-17a mRNA expression levels by quantitative reverse transcriptase PCR (RT-PCR). To this end, EL4 cells were treated with 10 μM of **3**, **25**, and **23** for 24 h before IL-17a mRNA levels were measured (Figure 6). The most potent isoxazole in vitro, **25**, significantly reduced IL-17a mRNA expression 27-fold, while the weaker inverse agonist **23** showed a smaller reduction (3.6-fold) compared to the DMSO control. As expected, **3** led to the most significant decrease in IL-17a expression (48-fold) which was in line with previous reports. This result demonstrates that the allosteric modulation of RORγt by optimized trisubstituted isoxazoles leads to an effective cellular response, correlating with the biochemical protein binding data and which is known to be beneficial for the treatment of autoimmune disease.[10−12]

2.8. Absorption, Distribution, Metabolism, and Excretion (ADME) Profile. To further assess the potential of **25** and isoxazole analogues such as **23** and **8**, we investigated the ADME profile of these compounds and compared them to indazole **3** (Table 5). The isoxazole compounds showed favorable profiles compared to **3** in terms

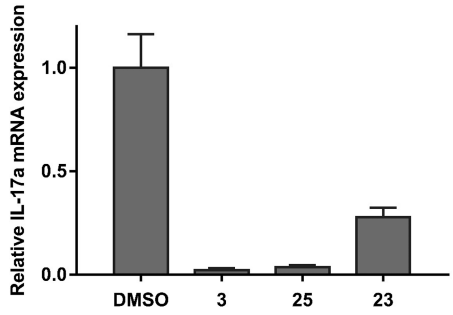


Figure 6. IL-17a mRNA expression in EL4 cells treated with ligand **3**, **25**, and **23** (10 μM, 24h) or DMSO. The level of IL-17a expression was normalized to that of the GAPDH expression. All data are expressed as the mean ± s.d. (n = 3). The relative gene expression was calculated by the $2^{-\Delta\Delta Ct}$ (Livak) method using the DMSO control as calibrator.

of chemical stability, solubility, and permeability through artificial plasma membranes (PAMPA). A metabolic stability study with human liver microsomes indicated that the 4-methylamino isoxazoles **23** and **25** were more liable to phase 1 metabolism compared to indazole **3**, which showed good stability. **23** and **25** showed promising phase 2 stability. In blood plasma, while inferior to **3**, the stability of **23** and **25** was acceptable, although all these compounds showed high levels of binding to plasma proteins. Pleasingly, the 5-phenyl-4-amido isoxazole **8** showed a good ADME profile, with comparable microsomal stability to **3** and reduced plasma protein binding. This likely indicates that further optimization of the C-4 and C-5 isoxazole substituents has the potential to produce candidate molecules with desirable in vivo efficacy.

3. CONCLUSIONS

To summarize, we report the design, synthesis, and early optimization of a novel class of RORγt allosteric inverse agonists. The chemotype of the central aromatic ring system differs significantly from all the other fused bicyclic ring systems reported thus far. To identify this novel, more diverse, molecular scaffold, we used the crystal structure of **3** bound to the RORγt allosteric site as the basis for a 3D pharmacophore screen against a virtual compound library. Rational design steps led to the discovery of the in silico designed hit **8**, which already featured a modest inhibition of transcriptional coactivator recruitment to the RORγt LBD and served as a starting point for further optimization in a SAR campaign. A second and highly efficient iteration of lead optimization was guided by in silico docking. Through the synthesis of just five derivatives (Table 2), this process delivered **25** (**FM26**), a submicromolar allosteric inverse agonist. It is highly noteworthy that there was a strong correlation between the Glide dockings scores and the RORγt biochemical activity within this new class of isoxazole. Whereas screening approaches do not overtly identify allosteric ligands, our rational scaffold hopping approach is much more targeted, with less demand on experimental resource. Overall, the discovery workflow adopted, with a central role for structure-driven in silico screening and optimization, showed to be highly effective and might have wider application in expediting NR allosteric drug discovery.

Competitive coactivator recruitment and ligand binding assays were used to confirm the allosteric mode-of-action, with concomitant cooperative RORγt binding with an inverse

DOI: 10.1021/acs.jmedchem.9b01372
J. Med. Chem. 2020, 63, 241−259

Table 5. ADME Properties for Ligands 3, 8, 23, and 25

compound	chemical stability (% remain)	solubility (μM)	PAMPA (% flux)	microsomal stability: phase 1 (CL_{int}, μL/min/mg)	microsomal stability: phase 2 (% remain)	plasma stability (% remain)	plasma protein binding (% bound)
3	81.0	390	23.7	−1.2	47.1	100	99.9
8	95.4	490	60.1	−0.1	100	99.9	97.8
23	100	392	50.4	43.2	92.8	86.5	100
25	95.3	411	33.6	20.7	69.8	85.9	99.9

agonist. This was also shown for thienopyrrazole **5**, having not previously been disclosed. The cocrystal structure of **25** in complex with the RORγt LBD unequivocally proved the allosteric binding mode, via a similar mechanism to **3** and was impressively similar to the initially docked structure of **25** in RORγt. The cocrystal of **25** with the RORγt LBD revealed a number of unique interactions and structural RORγt modifications that bring forward intriguing insights and new lines of exploration regarding RORγt allosteric ligand binding, selectivity, and affinity optimization, which are currently explored. Compound **25** was shown to significantly reduce IL-17a mRNA expression in EL4 cells and to have a promising ADME profile. These factors highlight the potential of this new isoxazole-based ligand class and overt targeting of the RORγt allosteric site to deliver effective treatments for autoimmune diseases.

4. EXPERIMENTAL SECTION

4.1. Pharmacophore Screening. The receptor−ligand complex structure (PDB code: 4YPQ) was prepared using the Protein Preparation Wizard within Maestro (version 2017−2, Schrödinger LLC, New York, NY, USA) (default parameters). A 3D pharmacophore model for **3** bound to the allosteric pocket of RORγt LBD was created using Phase (version 2017-2, Schrödinger LLC, default hypothesis settings). Energy minimized 3D ligand conformations for each molecule to be investigated were generated using the Ligand Preparation wizard within Maestro (default parameters). These were screened against the hypothesis whereby up to 50 ligand conformations were generated for each molecule. A hit was returned for compounds that matched 4 out of 6 pharmacophore features, and these were ranked using the Phase Screen Score. The structure and ranking for the top 30 hits identified from the Asinex Gold Platinum library can be found in the Supporting Information.

4.2. Molecular Docking Studies. The receptor−ligand structure (PDB code: 4YPQ) was prepared as described above. A receptor grid centered on the bound ligand was created using Glide (version 2017-2, Schrödinger LLC). All parameters were kept as the default. Ligand libraries were either enumerated in SMILES format using the open-access Chem-T software or generated manually (see the Supporting Information). Ligands were prepared using the Ligand Preparation wizard as described above. Ligands were docked using Glide (version 2017-2, Schrödinger LLC) in standard precision mode with flexible ligand sampling. The predicted binding modes of all ligands were ranked according to their Glide Score (see Supporting Information for selected examples).

4.3. General Chemistry. All nonaqueous reactions were performed under an argon atmosphere unless otherwise stated. Water-sensitive reactions were performed in oven-dried glassware, cooled under argon before use. Solvents were removed in vacuo using a Büchi rotary evaporator and a diaphragm pump. THF and CH_2Cl_2 were dried and purified by means of a MBRAUN Solvent Purification System (MB-SPS-800). Anhydrous DMF was obtained in SureSeal bottles from Sigma-Aldrich. All other solvents used were of chromatography or analytical grade and supplied by Biosolve or Sigma-Aldrich. Commercially available starting materials were obtained from Sigma-Aldrich, Fluka, Acros, Alfa-Aesar, or Fluorochem and were used without further purification unless stated. TLC was carried out on aluminum-backed silica (Merck silica gel 60 F254) plates supplied by Merck. Visualization of the plates was achieved using an ultraviolet lamp (λ_{max} = 254 nm), $KMnO_4$, anisaldehyde, or ninhydrin. Column chromatography was either performed manually using silica gel (60−63 um particle size) or using an automated Grace Reveleris X2 chromatograph with prepacked silica columns supplied by Buchi/Grace (40 μm particle size). LC−MS analysis was carried out with a system comprising a Thermo Fischer LCQ Fleet Ion Trap Mass Spectrometer and C18 Jupiter SuC4300A 150 × 2.0 mm column using a gradient of 5−100% MeCN in water (+ 0.1% HCOOH) over 15 min. The purity of the samples was assessed using a UV detector at 254 nm. Unless otherwise stated all final compounds were >95% pure as judged by HPLC. GCMS analysis was performed on a Phenomenex Zebron ZB-5MS 30 m × 0.25 mm × 0.25 mm column with a gradient of 80 °C for 1 min to 300 °C for 1 min with a rate of 30 °C/min in helium gas connected to a GCMS-QP2010 Plus Quadrupole Mass Spectrometer. High resolution mass spectra (HRMS) were recorded using a Waters ACQUITY UPLC I-Class LC system coupled to a Xevo G2 Quadrupole Time of Flight (Q-tof) mass spectrometer. Proton (^{1}H) and carbon (^{13}C) NMR spectral data were collected on a 400 MHz Bruker Cryomagnet or 400 MHz Varian Gemini. Chemical shifts (δ) are quoted in parts per million (ppm) and referenced to the residual solvent peak. Coupling constants (J) are quoted in Hertz (Hz) and splitting patterns reported in an abbreviated manner: app. (apparent), s (singlet), d (doublet), t (triplet), q (quartet), and m (multiplet). Assignments were made with the aid of 2D COSY, HMQC, and HMBC experiments.

4.3.1. General Procedure for Ester Hydrolysis. $LiOH{\cdot}H_2O$ (5.0 equiv) was added to a suspension of ester (1.0 equiv) in a 4:1 mixture of MeOH-H_2O (0.2 M). The reaction mixture was heated to 70 °C until TLC analysis indicated complete consumption of the starting material. MeOH was removed in vacuo, and the resulting aqueous mixture was acidified to pH 3 using 10% v/v aqueous HCl and extracted with a 9:1 mixture of CH_2Cl_2-MeOH (× 5). The combined organic phase was dried ($MgSO_4$), filtered, and concentrated in vacuo to furnish an ester which was purified as described.

4.3.2. General Procedure for Amide Coupling. Carboxylic acids (1.0 equiv) were dissolved in $SOCl_2$ (50 equiv) and heated to 50 °C for 2 h. The excess $SOCl_2$ was removed in vacuo to furnish an acid chloride intermediate that was immediately dissolved in CH_2Cl_2 (0.1 M). To this was added NEt_3 (3.0 equiv), the appropriate amine or aniline (1.5 equiv), and DMAP (0.1 equiv), and the reaction mixture was stirred at reflux for 18 h. The reaction mixture was diluted with saturated aqueous NH_4Cl solution and extracted with ethyl acetate (3×). The combined organic phase was washed with brine, dried over $MgSO_4$, filtered, and concentrated in vacuo. The crude product was purified by flash column chromatography (SiO_2) using the specified eluent.

4.3.3. General Procedure for tert-Butyl Ester Deprotection. Esters (1.0 equiv) were treated with a 20% trifluoroacetic acid solution in CH_2Cl_2 (0.2 M). The reaction mixture was stirred at the specified temperature for the specified amount of time and then concentrated in vacuo. The crude product was purified as indicated.

4.3.4. General Procedure for Suzuki Coupling. Under an inert atmosphere, the pinacol boronate (2.0 equiv), Cs_2CO_3 (2.0 equiv), and $Pd(dppf)Cl_2$ (0.1 equiv) were added to a solution of bromide **30a** (1.0 equiv) in degassed DME. The reaction mixture was heated at 85 °C for 8 h, cooled to room temperature, diluted with saturated

DOI: 10.1021/acs.jmedchem.9b01372
J. Med. Chem. 2020, 63, 241−259

aqueous NH_4Cl, and extracted with EtOAc (3×). The combined organic phase was dried ($MgSO_4$), filtered, and concentrated in vacuo. The crude product was purified by flash column chromatography using the specified eluent.

4.3.5. General Procedure for Conversion of Esters to Aldehydes. $LiAlH_4$ (1 M in THF, 1.0 equiv) was added dropwise to a solution of ester (1.0 equiv) in THF (0.2 M) at 0 °C. The reaction mixture was warmed to room temperature and stirred until TLC analysis indicated complete consumption of the starting material. The reaction mixture was cooled to 0 °C, quenched by the addition of saturated aqueous NH_4Cl solution, and extracted with EtOAc (3×). The combined organic phase was dried ($MgSO_4$), filtered, and concentrated in vacuo. The resulting intermediate product was dissolved in CH_2Cl_2 (0.2 M). To this was added Dess-Martin Periodinane (1.5 equiv), and the reaction mixture was stirred at room temperature until TLC analysis indicated complete consumption of the intermediate. The reaction mixture was quenched by the addition of 10% aqueous $Na_2S_2O_3$ solution and extracted with CH_2Cl_2 (3×). The combined organic phase was washed with saturated aqueous $NaHCO_3$ and H_2O, dried ($MgSO_4$), filtered, and concentrated in vacuo to furnish the title compound which was purified as described.

4.3.6. General Procedure for Reductive Amination. The chosen amine or aniline (1.0 equiv) was added to a solution of the appropriate aldehyde (1.0 equiv) and AcOH (0.1 equiv) in MeOH or EtOH (0.25 M). The reaction mixture was heated at reflux for 24 h and then concentrated in vacuo. The intermediate imine was isolated by flash column chromatography using the specified eluent and then dissolved in MeOH or EtOH (0.2 M), cooled to 0 °C (ice), and treated with $NaBH_4$ (5.0 equiv). The reaction mixture was held at the specified temperature until TLC analysis indicated complete consumption of the imine. The solvent was removed in vacuo, and the mixture was dissolved in CH_2Cl_2 and washed with water. The aqueous phase was further extracted with CH_2Cl_2 (2×), dried ($MgSO_4$), filtered, and concentrated in vacuo. The crude product was purified by flash column chromatography (SiO_2) using the specified eluent.

*4.3.7. 4-{3-[2-Chloro-6-(trifluoromethyl)phenyl]-5-methyl-1,2-oxazole-4-amido}benzoic Acid (**7**).* According to the General Procedure for amide coupling, carboxylic acid **11a** (60.0 mg, 0.199 mmol) was coupled with *tert*-butyl-4-amino benzoate. The crude product was purified by flash column chromatography, eluting with 20% EtOAc in cyclo-hexane, to furnish the amide (46.0 mg, 48%). The intermediate product (43.0 mg, 0.089 mmol) was subject to *tert*-butyl ester deprotection (see General Procedure for tert-Butyl Ester Deprotection) and purified by trituation with Et_2O to furnish **7** (33.0 mg, 87%) as a colorless solid. R_f = 0.52 (9:1 CH_2Cl_2-MeOH); ^1H NMR (400 MHz, MeOD): δ (ppm) 7.97 (2 H, d, J = 8.8, benzoate H-2), 7.81 (2 H, app. d, J = 8.0, Ar H-3 and Ar H-5), 7.67 (1 H, t, J = 8.0, Ar H-4), 7.61 (2 H, d, J = 8.8, benzoate H-3), 2.76 (3 H, s, CH_3); ^{13}C NMR (100 MHz, MeOD): δ (ppm) 171.3 (C-5), 161.2 (CO_2H), 159.5 (C-3), 143.8 (benzoate C-4), 137.4 (ArC-2), 134.4 (ArC-3), 132.7 (q, J = 30.9, ArC-6), 132.6 (ArC-4), 131.8 (benzoate C-2), 127.6 (ArC-1), 127.5 (benzoate C-1), 126.1 (q, J = 5.1, ArC-5), 120.6 (benzoate C-3), 116.1 (C-4), 12.8 (CH_3); LC–MS (ESI): calcd for $C_{19}H_{13}ClF_3N_2O_4$ $[M + H]^+$: 425.04, observed: 425.17, LC R_t: 6.22 min. HRMS (ESI): calc. for $C_{19}H_{13}ClF_3N_2O_4$ $[M + H]^+$: 425.0516, observed: 425.0511.

*4.3.8. 4-{3-[2-Chloro-6-(trifluoromethyl)phenyl]-5-phenyl-1,2-oxazole-4-amido}benzoic Acid (**8**).* *tert*-Butyl benzoate **14** (30.0 mg, 0.055 mmol) was deprotected according to the General Procedure for *tert*-butyl ester deprotection. The crude product was purified by trituation with Et_2O to furnish **8** (21.0 mg, 78%) as a colorless solid. R_f = 0.55 (9:1 CH_2Cl_2-MeOH); ^1H NMR (400 MHz, DMSO-d_6): δ (ppm) 7.97 (1 H, d, J = 8.2, ArH-3 or ArH-5), 7.92 (1 H, d, J = 7.9, ArH-3 or ArH-5), 7.85–7.83 (4 H, m, benzoate H-2, PhH-ortho), 7.78 (1 H, app. t, J = 8.1, ArH-4), 7.58–7.54 (5 H, m, benzoate H-3, PhH-meta, PhH-para); ^{13}C NMR (100 MHz, $CDCl_3$): δ (ppm) 167.0 (C-5), 166.8 (CO_2H), 158.9 (CO_2NH), 158.7 (C-3), 142.3 (benzoate C-4), 135.5 (ArC-2), 133.7 (ArC-3), 132.4 (PhC-quart.), 131.6 (ArC-4), 130.6 (ArC-6), 130.3 (benzoate C-2), 129.4 (PhC-ortho), 127.3 (PhC-meta), 126.0 (PhC-para), 125.9 (benzoate C-1), 125.3 (ArC-5 and ArC-1), 119.3 (benzoate C-3), 113.4 (C-4), quartet for CF_3 not observed; LC–MS (ESI): calcd for $C_{24}H_{15}ClF_3N_2O_4$ $[M + H]^+$: 487.06, observed: 487.17, LC R_t: 7.00 min. HRMS (ESI): calcd for $C_{24}H_{15}ClF_3N_2O_4$ $[M + H]^+$: 487.0672, observed: 487.0662.

*4.3.9. (E)-N-{[2-Chloro-6-(trifluoromethyl)phenyl]methylidene}-hydroxylamine (**9**).* Hydroxylamine hydrochloride (3.95 g, 57.0 mmol, 1.2 equiv) was suspended in EtOH (20 mL) and 10% w/v aqueous solution of NaOH (20 mL) was added such that the final pH of the resulting solution was < pH 9. 2-Chloro-6-(trifluoromethyl)-benzaldehyde (9.88 g, 47.4 mmol, 1.0 equiv) was then added as a solution in EtOH (20 mL) and the mixture was stirred at room temperature for 18 h. The reaction mixture was diluted with H_2O (100 mL) and extracted with CH_2Cl_2 (3 × 100 mL). The combined organic phase was dried ($MgSO_4$), filtered, and concentrated in vacuo to furnish **9** (8.77 g, 83%) as a colorless solid which was used without further purification. R_f = 0.45 (4:1 c-hexane-EtOAc); ^1H NMR (400 MHz, $CDCl_3$): δ (ppm) 8.97 (1H, s, N=C*H*), 8.36 (1H, s, NO*H*), 7.67–7.64 (2 H, m, H-3, H-5), 7.45 (1 H, app. t, J = 8.0, H-4); ^{13}C NMR (100 MHz, $CDCl_3$): δ (ppm) 145.3 (N=*C*H), 135.7 (C-2), 133.6 (C-3), 131.3 (q, J = 31.2, C-6), 130.2 (C-4), 129.0 (C-1), 125.1 (q, J = 5.5, C-5), 123.22 (q, J = 274.2, F_3C); LC–MS (ESI): calcd for $C_8H_6ClF_3NO$ $[M + H]^+$: 224.00, observed: 224.00, LC R_t: 5.82 min.

*4.3.10. (Z)-2-Chloro-N-hydroxy-6-(trifluoromethyl)benzene-1-carbonimidoyl Chloride (**9a**).* *N*-Chlorosuccinamide (5.22 g, 39.1 mmol, 1.0 equiv) was added to a solution of hydroxylamine **9** (8.74 g, 39.1 mmol, 1.0 equiv) in DMF (80 mL). The reaction mixture was stirred at 60 °C for 18 h then diluted with H_2O (150 mL) and extracted with Et_2O (3 × 100 mL). The combined organic phase was washed with H_2O (3 × 100 mL) and brine (100 mL), dried ($MgSO_4$), filtered, and concentrated in vacuo to furnish **9a** (9.10 g, 95% purity, 86%) which was used immediately in the next step without further purification. R_f = 0.42 (4:1 c-hexane-EtOAc); ^1H NMR (400 MHz, $CDCl_3$): δ (ppm) 8.50 (1H, s, NO*H*), 7.68–7.66 (2 H, m, H-3, H-5), 7.53 (1 H, app. t, J = 8.1, H-4).

*4.3.11. Ethyl 3-[2-Chloro-6-(trifluoromethyl)phenyl]-5-methyl-1,2-oxazole-4-carboxylate (**10a**).* NEt_3 (0.570 mL, 4.07 mmol, 2.5 equiv) was added to a solution of imidoyl chloride **9a** (0.421 g, 1.63 mmol, 1.0 equiv) in THF (2.5 mL). A white precipitate formed immediately after which was added ethyl 2-butynoate (0.190 mL, 1.63 mmol, 1.0 equiv). The reaction mixture was heated to reflux for 4 h, filtered, and concentrated in vacuo. The crude material was purified by automated flash column chromatography, eluting with a gradient of 2–5% EtOAc in c-hexane, to furnish **10a** (0.375 g, 69%) as a colorless oil. R_f = 0.22 (9:1 c-hexane-EtOAc); ^1H NMR (400 MHz, $CDCl_3$): δ (ppm) 7.69 (1 H, d, J = 8.0, ArH-3 or ArH-5), 7.66 (1 H, d, J = 8.0, ArH-3 or ArH-5), 7.53 (1 H, app. t, J = 8.0, ArH-4); 4.07 (2 H, 2× dq (overlapping), J = 12.7, 7.1, $CO_2CH_2CH_3$), 2.78 (3 H, s, CH_3), 0.98 (3 H, t, J = 7.1, OCH_2CH_3); ^{13}C NMR (100 MHz, $CDCl_3$): δ (ppm) 175.4 (C-5), 161.1 (CO_2Et), 158.1 (C-3), 136.3 (ArC-2), 132.7 (ArC-3), 131.6 (q, J = 31.6, ArC-6), 130.6 (ArC-4), 127.5 (ArC-1), 124.6 (q, J = 5.0, ArC-5), 123.0 (q, J = 274.5, F_3C), 110.2 (C-4), 60.6 (OCH_2CH_3), 13.66 (CH_3), 13.3 (OCH_2CH_3); LC–MS (ESI): calcd for $C_{14}H_{12}ClF_3NO_3$ $[M + H]^+$: 334.04, observed: 334.08, LC R_t: 7.47 min.

*4.3.12. Ethyl 3-[2-Chloro-6-(trifluoromethyl)phenyl]-5-phenyl-1,2-oxazole-4-carboxylate (**10b**).* NEt_3 (3.92 mL, 28.1 mmol, 2.5 equiv) was added to a solution of imidoyl chloride **9a** (2.90 g, 11.3 mmol, 1.0 equiv) in THF (17 mL). A white precipitate formed immediately after which was added ethyl-3-phenyl propionate (1.85 mL, 11.3 mmol, 1.0 equiv). The reaction mixture was heated to reflux for 6 h, filtered, and concentrated in vacuo. The crude material was purified by automated flash column chromatography, eluting with a gradient of 0–25% EtOAc in *n*-heptane, to furnish **10b** (3.59 g, 80%) as a colorless solid. R_f = 0.47 (4:1 c-hexane-EtOAc); ^1H NMR (400 MHz, $CDCl_3$): δ (ppm) 8.16–8.13 (2 H, m, PhH-ortho), 7.74 (1 H, d, J = 7.9, ArH-3 or ArH-5), 7.71 (1 H, d, J = 8.2, H-3 or H-5), 7.59–7.51 (4 H, m, H-4, Ar–H), 4.06 (2 H, dq (2 overlapping), J = 11.8, 7.1, $CO_2CH_2CH_3$), 0.88 (3 H, t, J = 7.1, OCH_2CH_3); ^{13}C NMR (100 MHz, $CDCl_3$): δ (ppm) 173.0 (C-5), 160.8 (CO_2Et), 159.2 (C-3),

DOI: 10.1021/acs.jmedchem.9b01372
J. Med. Chem. 2020, 63, 241–259

136.3 (ArC-2), 132.6 (ArC-3), 131.7 (PhC-quart.), 131.5 (q, J = 30.5, ArC-6), 130.5 (ArC-4), 129.2 (PhC-ortho), 128.5 (PhC-meta), 127.8 (q, J = 1.8, ArC-1), 126.3 (PhC-meta), 124.5 (q, J = 5.0, ArC-5), 122.9 (q, J = 274.3, F_3C), 109.3 (C-4), 60.8 (OCH_2CH_3), 13.3 (OCH_2CH_3); LC−MS (ESI): calcd for $C_{19}H_{14}ClF_3NO_3$ $[M + H]^+$: 396.06, observed: 396.17, LC R_t: 8.40 min.

*4.3.13. 3-[2-Chloro-6-(trifluoromethyl)phenyl]-5-methyl-1,2-oxazole-4-carboxylic acid (**11a**).* According to the General Procedure for ester hydrolysis, ester **10a** (0.273 g, 0.820 mmol) was hydrolyzed in 8 h to furnish **11a** (0.210 g, 84%) as a colorless solid which required no further purification. R_f = 0.61 (EtOAc); ^{1}H NMR (400 MHz, DMSO-d_6): δ (ppm) 13.09 (1 H, br. s, CO_2H), 7.96 (1 H, d, J = 8.0, ArH-3 or ArH-5), 7.90 (1 H, d, J = 8.0, ArH-3 or ArH-5), 7.77 (1 H, app. t, J = 8.0, ArH-4), 2.76 (3 H, s, CH_3); ^{13}C NMR (100 MHz, DMSO-d_6): δ (ppm) 175.3 (C-5), 161.9 (CO_2H), 158.2 (C-3), 135.3 (ArC-2), 133.4 (ArC-3), 131.8 (ArC-4), 130.1 (q, J = 30.8, ArC-6), 126.8 (ArC-1), 125.1 (q, J = 5.0, ArC-5), 123.0 (q, J = 274.4, F_3C), 110.5 (C-4), 12.8 (CH_3); LC−MS (ESI): calcd for $C_{12}H_6ClF_3NO_3$ $[M-H]^-$: 304.01, observed: 304.17, LC R_t: 5.82 min.

*4.3.14. 3-[2-Chloro-6-(trifluoromethyl)phenyl]-5-phenyl-1,2-oxazole-4-carboxylic acid (**11b**).* According to the General Procedure for ester hydrolysis, ester **10b** (3.66 g, 9.26 mmol) was hydrolyzed in 8 h to furnish **11b** (3.25 g, 95%) as a colorless solid which required no further purification. R_f = 0.35 (1:1 c-hexane-EtOAc); ^{1}H NMR (400 MHz, $CDCl_3$): δ (ppm) 8.05−8.03 (2 H, m, PhH-ortho), 7.71(1 H, d, J = 8.0, ArH-3 or ArH-5), 7.68 (1 H, d, J = 8.1, H-3 or H-5), 7.60−7.50 (4 H, m, H-4, Ar−H); ^{13}C NMR (100 MHz, DMSO-d_6): δ (ppm) 171.8 (C-5), 161.5 (CO_2H), 159.3 (C-3), 135.2 (ArC-2), 133.4 (ArC-3), 132.0 (PhC-quart.), 131.8 (ArC-4), 130.0 (q, J = 30.5, ArC-6), 129.0 (PhC-ortho), 128.7 (PhC-meta), 126.7 (ArC-1), 125.7 (PhC-meta), 125.2 (q, J = 5.0, ArC-5), 123.0 (q, J = 274.4, F_3C), 99.4 (C-4); LC−MS (ESI): calcd for $C_{17}H_{10}ClF_3NO_3$ $[M + H]^+$: 368.02, observed: 368.08, LC retention time: 7.03 min. HRMS (ESI): calcd for $C_{17}H_{10}ClF_3NO_3$ $[M + H]^+$: 368.0301, observed: 368.0299.

*4.3.15. 3-[2-Chloro-6-(trifluoromethyl)phenyl]-5-phenyl-1,2-oxazole-4-carbaldehyde (**12**).* Carboxylic acid **11b** (2.0 g, 5.44 mmol,1.0 equiv) was dissolved in $SOCl_2$ (10.0 mL, 138 mmol, 25 equiv) and heated to 60 °C for 2 h. Excess $SOCl_2$ was removed in vacuo, and the intermediate acid chloride was immediately dissolved in CH_2Cl_2 (20 mL) and cooled to 0 °C. To this was added NEt_3 (2.27 mL, 16.3 mmol, 3.0 equiv) and *N,O*-dimethyl hydroxylamine hydrochloride (0.580 g, 5.98 mmol, 1.1 equiv). The reaction mixture was allowed to warm to room temperature with stirring over 16 h before being quenched by the addition of saturated aqueous NH_4Cl solution and extracted with CH_2Cl_2 (3 × 20 mL). The combined organic phase was dried ($MgSO_4$), filtered, and concentrated in vacuo. The resulting Weinreb amide was dissolved in THF (20 mL) and cooled to 0 °C. To this was added $LiAlH_4$ (1 M in THF, 2.72 mL, 2.72 mmol, 0.5 equiv), and the reaction mixture was stirred at 0 °C for 1 h before being quenched by the addition of saturated aqueous NH_4Cl solution (20 mL) and extracted with EtOAc (3 × 20 mL). The combined organic phase was dried ($MgSO_4$), filtered, and concentrated in vacuo to furnish a crude product which was purified by automated flash column chromatography, eluting with a gradient of 10−30% EtOAc in *n*-heptane, to furnish **12** (1.25 g, 65%) as a colorless solid. R_f = 0.65 (1:1 c-hexane-EtOAc); ^{1}H NMR (400 MHz, $CDCl_3$): δ (ppm) 9.93 (1 H, s, CHO), 8.06−8.04 (2 H, m, PhH-ortho), 7.77 (1 H, d, J = 7.9, ArH-3 or ArH-5), 7.74 (1 H, d, J = 7.8, ArH-3 or ArH-5), 7.68−7.59 (4 H, m, H-4, PhH); ^{13}C NMR (100 MHz, $CDCl_3$): δ (ppm) 182.8 (CHO), 174.6 (C-5), 160.8 (CO_2Et), 158.6 (C-3), 136.3 (ArC-2), 133.2 (ArC-3), 132.7 (PhC-quart.), 132.0 (q, J = 30.9, ArC-6), 131.3 (ArC-4), 129.5 (PhC-ortho), 128.9 (PhC-meta), 125.9 (ArC-1), 125.7 (PhC-para), 125.0 (ArC-5), 123.0 (q, J = 274.9, F_3C), 116.2 (C-4); LC−MS (ESI): calcd for $C_{17}H_{10}ClF_3NO_2$ $[M + H]^+$: 352.03, observed: 352.08, LC R_t: 7.28 min.

*4.3.16. 3-[2-Chloro-6-(trifluoromethyl)phenyl]-5-phenyl-1,2-oxazol-4-amine (**13**).* NEt_3 (0.760 mL, 5.44 mmol, 1.1 equiv) and diphenylphosphoryl azide (1.06 mL, 4.95 mmol, 1.0 equiv) were added to a prewarmed solution of acid **11b** (1.82 g, 4.95 mmol, 1.0 equiv) in *t*-BuOH (18 mL) at 50 °C. The reaction mixture was then heated to 85 °C for 18 h after which it was cooled to room temperature and diluted with 1 M aqueous HCl (50 mL) and extracted with EtOAc (3 × 30 mL). The combined organic phase was washed with saturated aqueous $NaHCO_3$ (100 mL) and brine (100 mL), dried ($MgSO_4$), filtered, and concentrated in vacuo. The crude product was purified by automated flash column chromatography, eluting with a gradient of 0−20% EtOAc in *n*-heptane, to furnish a carbamate (1.41 g, 65%) as a colorless solid. Trifluoroacetic acid (3.0 mL) was added to a solution of the carbamate (1.13 g, 2.58 mmol, 1.0 equiv) in CH_2Cl_2 (9.0 mL). The reaction mixture was heated at reflux for 4 h then cooled to room temperature and concentrated in vacuo. The crude product was dissolved in CH_2Cl_2 (100 mL) and washed with saturated aqueous $NaHCO_3$ (100 mL) and water (100 mL), dried ($MgSO_4$), filtered, and concentrated in vacuo to furnish **13** (0.798 g, 91%) as a pale yellow solid that was used without further purification. R_f = 0.56 (1:1 c-hexane-EtOAc); ^{1}H NMR (400 MHz, $CDCl_3$): δ (ppm) 7.86 (1 H, d, J = 7.0, ArH-3 or ArH-5), 7.79−7.76 (2 H, m, PhH-ortho), 7.61 (1 H, app. t, J = 8.0, ArH-3 or ArH-5), 7.54−7.49 (3 H, m, PhH), 7.41 (1 H, app. t, J = 8.0, ArH-4), 2.97 (2 H, s, NH_2); ^{13}C NMR (100 MHz, $CDCl_3$): δ (ppm) 164.5 (C-5), 154.7 (C-3), 137.0 (ArC-2), 133.4 (ArC-3), 131.4 (PhC-quart.), 129.1 (PhC-ortho), 128.9 (9ArC-4), 128.3 (PhC-para), 126.5 (ArC-5), 126.0 (q, J = 4.0, ArC-1), 125.2 (PhC-meta), 122.9 (q, J = 274.4, CF_3), 110.4 (C-4); LC−MS (ESI): calcd for $C_{16}H_{11}ClF_3N_2O$ $[M + H]^+$: 339.04, observed: 339.08, LC R_t: 7.12 min.

*4.3.17. tert-Butyl 4-{3-[2-Chloro-6-(trifluoromethyl)phenyl]-5-phenyl-1,2-oxazole-4-amido}benzoate (**14**).* According to the General Procedure for amide coupling, carboxylic acid **11b** (0.200 g, 0.540 mmol) was coupled with *tert*-butyl-4-amino benzoate. The crude product was purified by flash column chromatography, eluting with 15% EtOAc in c-hexane, to furnish amide **14** (0.260 g, 88%) as a colorless solid. R_f = 0.55 (3:2 c-hexane-EtOAc); ^{1}H NMR (400 MHz, $CDCl_3$): δ (ppm) 7.96 (2 H, dd, J = 7.9, 1.7, PhH-ortho), 7.86 (2 H, d, J = 8.7, benzoate H-2), 7.77 (2 H, app. t, J = 8.1, ArH-3 and ArH-5), 7.63−7.56 (4 H, m, PhH-meta, PhH-para, ArH-4), 7.37 (1 H, br. s, C(O)NH), 7.29 (2 H, d, J = 8.7, benzoate H-3), 1.55 (9 H, s, $CO_2C(CH_3)_3$); ^{13}C NMR (100 MHz, $CDCl_3$): δ (ppm) 169.4 (C-5), 165.1 (CO_2H), 158.4 (C-3 and CO_2NH), 140.8 (benzoate C-4), 136.6 (ArC-2), 133.3 (ArC-3), 132.1 (PhC-quart.), 131.5 (ArC-4), 130.7 (ArC-6), 129.5 (PhC-ortho and benzoate C-2), 128.7 (PhC-meta), 128.2 (benzoate C-1), 126.2 (ArC-1), 126.0 (PhC-para), 125.1 (ArC-5), 118.7 (benzoate C-3), 113.0 (C-4), 81.1 ($CO_2C(CH_3)_3$), 28.3 ($CO_2C(CH_3)_3$), quartet for CF_3 not observed; LC−MS (ESI): calcd for $C_{28}H_{23}ClF_3N_2O_4$ $[M + H]^+$: 543.12, observed: 543.08, LC R_t: 8.88 min. HRMS (ESI): calcd for $C_{28}H_{23}ClF_3N_2O_4$ $[M + H]^+$: 543.1298, observed: 543.1292.

*4.3.18. 2-(4-{3-[2-Chloro-6-(trifluoromethyl)phenyl]-5-phenyl-1,2-oxazole-4-amido}phenyl) acetic acid (**15**).* According to the General Procedure for amide coupling, carboxylic acid **11b** (0.200 g, 0.540 mmol) was coupled with methyl-(4-aminophenyl) acetate. The crude product was purified by flash column chromatography, eluting with a gradient of 15−45% EtOAc in *n*-heptane, to furnish the amide (0.173 g, 62%). The intermediate product (0.117 g, 0.230 mmol) was subject to ester hydrolysis according to the General Procedure for ester hydrolysis and purified by trituation with Et_2O to furnish **15** (0.099 g, 87%) as a colorless solid. R_f = 0.55 (9:1 CH_2Cl_2-MeOH); ^{1}H NMR (400 MHz, DMSO-d_6): δ (ppm) 12.32 (1 H, br. s, CO_2H), 10.49 (1 H, s, CONH), 7.98 (1 H, d, J = 8.2, ArH-3 or ArH-5), 7.93 (1 H, d, J = 8.0, ArH-3 or ArH-5), 7.88−7.87 (2 H, m, PhH-ortho), 7.79 (1 H, app. t, J = 8.1, ArH-4), 7.61−7.59 (3 H, m, PhH-meta, PhH-para), 7.40 (2 H, d, J = 8.2, benzoate H-2), 7.15 (2 H, d, J = 8.2, benzoate H-3), 3.49 (2 H, br. s, benzylic CH_2); ^{13}C NMR (100 MHz, DMSO-d6): δ (ppm) 172.7 (CO_2H), 166.6 (C-5), 158.7 (CO_2NH), 158.4 (C-3), 136.9 (benzoate C-4), 135.5 (ArC-2), 133.6 (ArC-3), 132.3 (PhC-quart.), 131.4 (ArC-4), 130.9 (benzoate C-1), 130.5 (q, J = 30.9, ArC-6), 129.7 (benzoate C-2), 129.4 (PhC-ortho), 127.2 (PhC-meta), 126.0 (PhC-para), 125.5 (ArC-5), 125.3 (ArC-1), 122.9 (q, J = 274.5, CF_3), 119.9 (benzoate C-3), 113.8 (C-4), 30.7 (benzylic CH_2); LC−MS (ESI): calcd for $C_{25}H_{17}ClF_3N_2O_4$ $[M + H]^+$: 501.08,

DOI: 10.1021/acs.jmedchem.9b01372
J. Med. Chem. 2020, 63, 241−259

observed: 501.17, LC R_t: 6.67 min. HRMS (ESI): calcd for $C_{25}H_{17}ClF_3N_2O_4$ $[M + H]^+$: 501.0829, observed: 501.0829.

*4.3.19. 3-{3-[2-Chloro-6-(trifluoromethyl)phenyl]-5-phenyl-1,2-oxazole-4-amido}benzoic Acid (**16**).* According to the General Procedure for amide coupling, carboxylic acid **11b** (0.200 g, 0.540 mmol) was coupled with methyl-3-amino benzoate. The crude product was purified by flash column chromatography, eluting with 15% EtOAc in c-hexane, to furnish the amide (0.212 g, 78%). The intermediate product (0.100 g, 0.200 mmol) was subject to ester hydrolysis according to the General Procedure for ester hydrolysis and purified by trituation with Et_2O to furnish **16** (0.070 g, 72%) as a colorless solid. R_f = 0.51 (9:1 CH_2Cl_2-MeOH); ^{1}H NMR (400 MHz, DMSO-d_6): δ (ppm) 13.01 (1 H, br. s, CO_2H), 10.66 (1 H, s, CONH), 8.11 (1 H, s, benzoate H-2), 7.98 (1 H, d, J = 8.1, ArH-3 or ArH-5), 7.91 (1 H, d, J = 7.7, ArH-3 or ArH-5), 7.87 (2 H, m, PhH-ortho), 7.80 (1 H, app. t, J = 8.0, ArH-4), 7.68−7.64 (2 H, m, benzoate H-4 and H-6), 7.63−7.59 (3 H, m, PhH-meta, PhH-para), 7.40 (1 H, app. t, J = 7.8, benzoate H-5); ^{13}C NMR (100 MHz, DMSO-d_6): δ (ppm) 166.9 (C-5), 158.7 (CO_2H), 158.6 (CO_2NH), 154.5 (C-3), 138.5 (benzoate C-3), 135.4 (ArC-2), 133.6 (ArC-3), 132.4 (PhC-quart.), 131.5 (ArC-4), 129.4 (PhC-ortho), 129.0 (benzoate C-5), 127.3 (PhC-meta), 125.9 (PhC-para and benzoate C-1), 125.4 (ArC-5 and ArC-1), 124.9 (benzoate C-6), 124.0 (benzoate C-4), 120.6 (benzoate C-2), 113.5 (C-4), (quartet for CF_3 not observed); LC−MS (ESI): calcd for $C_{24}H_{15}ClF_3N_2O_4$ $[M + H]^+$: 487.06, observed: 487.25, LC R_t: 7.10 min. HRMS (ESI): calcd for $C_{24}H_{15}ClF_3N_2O_4$ $[M + H]^+$: 487.0672, observed: 487.0667.

*4.3.20. 4-{3-[2-Chloro-6-(trifluoromethyl)phenyl]-5-phenyl-1,2-oxazole-4-amido}-2-fluorobenzoic Acid (**17**).* According to the General Procedure for amide coupling, carboxylic acid **11b** (0.200 g, 0.540 mmol) was coupled with methyl-4-amino-2-fluoro benzoate. The crude product was purified by flash column chromatography, eluting with a gradient of 20−25% EtOAc in *n*-heptane, to furnish the amide (0.075 g, 27%). The intermediate product (0.063 g, 0.120 mmol) was subject to ester hydrolysis according to the General Procedure for ester hydrolysis and purified by trituation with Et_2O to furnish **17** (0.053 g, 87%) as a colorless solid. R_f = 0.27 (1:1 n-heptate-EtOAc); ^{1}H NMR (400 MHz, DMSO-d_6): δ (ppm) 13.05 (1 H, br. s, CO_2H), 10.94 (1 H, s, CONH), 7.99 (1 H, d, J = 8.2, ArH-3 or ArH-5), 7.94 (1 H, d, J = 7.9, ArH-3 or ArH-5), 7.87−7.78 (4 H, m, PhH-ortho, ArH-4, benzoate H-6), 7.62−7.59 (3 H, m, PhH-meta, PhH-para), 7.51 (1 H, d, J 13.1, benzoate H-3), 7.28 (1 H, d, J 8.7, benzoate H-5); ^{13}C NMR (100 MHz, DMSO-d6): δ (ppm) 167.3 (C-5), 164.5 (CO_2H), 161.5 (d, J = 256.0, benzoate C-2), 159.1 (CO_2NH), 158.7 (C-3), 143.6 (d, J = 11.4, benzoate C-4), 135.4 (ArC-2), 133.7 (ArC-3), 132.8 (benzoate C-6), 132.4 (PhC-quart.), 131.7 (ArC-4), 130.4 (q, J = 30.6, ArC-6), 129.4 (PhC-ortho), 127.4 (PhC-meta), 125.7 (PhC-para), 125.4 (ArC-5), 125.1 (ArC-1), 122.9 (q, J = 274.6, CF_3), 115.0 (benzoate C-5), 114.2 (d, J = 10.1, benzoate C-1), 113.1 (C-4), 107.2 (d, J = 27.5, benzoate C-3); LC−MS (ESI): calcd for $C_{24}H_{14}ClF_4N_2O_4$ $[M + H]^+$: 505.05, observed: 505.25, LC R_t: 7.10 min. HRMS (ESI): calcd for $C_{24}H_{14}ClF_4N_2O_4$ $[M + H]^+$: 505.0578, observed: 505.0569.

*4.3.21. 4-[({3-[2-Chloro-6-(trifluoromethyl)phenyl]-5-phenyl-1,2-oxazol-4-yl}formamido)methyl]benzoic Acid (**18**).* According to the General Procedure for amide coupling, carboxylic acid **11b** (0.200 g, 0.540 mmol) was coupled with methyl-4-aminomethyl benzoate. The crude product was purified by flash column chromatography, eluting with 15% EtOAc in cyclo-hexane, to furnish the amide (0.173 g, 62%). The intermediate product (0.106 g, 0.200 mmol) was subject to ester hydrolysis according to the General Procedure for ester hydrolysis and purified by trituation with Et_2O to furnish **18** (0.096 g, 96%) as a colorless solid. R_f = 0.51 (9:1 CH_2Cl_2-MeOH); ^{1}H NMR (400 MHz, MeOD): δ (ppm) 7.91 (2 H, d, J = 8.3, benzoate H-2), 7.84 (1 H, d, J = 7.7, ArH-3 or ArH-5), 7.83 (1 H, d, J = 8.3, ArH-3 or ArH-5), 7.78−7.76 (2 H, m, PhH-ortho), 7.72 (1 H, app. t, J = 8.0, ArH-4), 7.57−7.53 (1 H, m, PhH-para), 7.49−7.45 (2 H, m, PhH-meta), 7.24 (2 H, d, J = 8.3, benzoate H-3), 4.42 (1 H, d, J = 15.2, benzylic CHa), 4.40 (1 H, d, J = 15.2, benzylic CHb); ^{13}C NMR (100 MHz, DMSO-d6): δ (ppm) 167.2 (C-5), 166.6 (CO_2H), 160.0 (CO_2NH), 158.4 (C-3), 143.6 (benzoate C-4), 135.6 (ArC-2), 133.6 (ArC-3), 132.3 (PhC-quart.), 131.3 (ArC-4), 130.6 (q, J = 31.6, ArC-6), 129.5 (benzoate C-1), 129.2 (benzoate C-2 and PhC-ortho), 127.5 (PhC-meta), 127.4 (PhC-para), 125.9 (ArC-5), 125.4 (ArC-1), 122.9 (q, J = 274.1, CF_3), 118.8 (benzoate C-3), 113.6 (C-4), 42.4 (benzylic CH_2); LC−MS (ESI): calcd for $C_{25}H_{17}ClF_3N_2O_4$ $[M + H]^+$: 501.08, observed: 501.25, LC R_t: 6.67 min. HRMS (ESI): calcd for $C_{25}H_{17}ClF_3N_2O_4$ $[M + H]^+$: 501.0829, observed: 501.0818.

*4.3.22. 4-[({3-[2-Chloro-6-(trifluoromethyl)phenyl]-5-phenyl-1,2-oxazol-4-yl}methyl)amino] benzoic Acid (**19**).* Ethyl-4-aminobenzoate (86 mg, 0.52 mmol, 1.0 equiv)) and AcOH (0.5 mL) were added to a solution of aldehyde **12** (0.183 g, 0.520 mmol, 1.0 equiv) in EtOH (10.0 mL). The reaction mixture was heated at reflux for 4 h after which time it was cooled to room temperature and $NaCNBH_3$ (65.3 mg, 1.04 mmol, 2.0 equiv) was added. The reaction mixture was then heated at reflux for a further 12 h then concentrated in vacuo, diluted with EtOAc (10 mL) and washed with saturated aqueous $NaHCO_3$ (20 mL), water (20 mL), and brine (20 mL). The combined organic phase was dried ($MgSO_4$), filtered, and concentrated in vacuo. The crude product was purified by flash column chromatography, eluting with 17% EtOAc in *n*-heptane, to furnish the ester (81.4 mg, 31%). The intermediate product (0.049 g, 0.098 mmol) was subject to ester hydrolysis according to the General Procedure for ester hydrolysis and purified by trituation with Et_2O to furnish **19** (0.046 g, 99%) as a colorless solid. R_f = baseline (4:1 cyclo-hexane-EtOAc); ^{1}H NMR (400 MHz, DMSO-d_6): δ (ppm) 12.03 (1 H, br. s, CO_2H), 7.92−7.85 (4 H, m, ArH-3, ArH-5, PhH-ortho), 7.73 (1 H, app. t, J = 8.0, ArH-4), 7.64−7.58 (3 H, m, PhH-ortho and PhH-meta), 7.53 (2 H, d, J = 8.8, benzoate C-2), 6.48 (1 H, t, J = 5.3 CH_2NH), 6.37 (2 H, d, J = 8.8, benzoate H-3), 4.21 (1 H, dd, J = 14.7, 5.3, CH_aNH), 4.12 (1 H, dd, J = 14.7, 5.3, CH_bNH); ^{13}C NMR (100 MHz, DMSO-d6): δ (ppm) 167.4 (C-5), 166.4 (CO_2H), 159.6 (C-3), 151.6 (benzoate C-4), 135.5 (ArC-2), 133.7 (ArC-3), 132.2 (PhC-quart.), 130.8 (benzoate C-2), 130.7 (ArC-4), 130.6 (q, J = 30.4, ArC-6), 129.3 (PhC-ortho),127.2 (PhC-meta), 126.6 (PhC-para), 125.6 125.4 (ArC-5), 125.4 (q, J = 5.0, ArC-1), 122.9 (q, J = 274.6, CF_3), 117.6 (benzoate C-1), 113.1 (C-4), 110.7 (benzoate C-3), 35.7 (CH_2NH); LC−MS (ESI): calcd for $C_{24}H_{17}ClF_3N_2O_3$ $[M + H]^+$: 473.08, observed 473.00, LC R_t: 7.35 min. HRMS (ESI): calcd for $C_{24}H_{17}ClF_3N_2O_3$ $[M + H]^+$: 473.0880, observed: 473.0862.

*4.3.23. 4-({3-[2-Chloro-6-(trifluoromethyl)phenyl]-5-phenyl-1,2-oxazol-4-yl}carbamoyl) Benzoic Acid (**20**).* According to the General Procedure for amide coupling, monomethyl terephthalate (23.0 mg, 0.120 mmol) was coupled with amine **13** (43.0 mg, 0.120 mmol). The crude product was purified by flash column chromatography, eluting with 25% EtOAc in c-hexane, to furnish the amide (46.0 mg, 76%). The intermediate product (35.0 mg, 0.070 mmol) was subject to ester hydrolysis according to the General Procedure for ester hydrolysis and purified by trituation with Et_2O to furnish **20** (22.6 mg, 66%) as a colorless solid. R_f = 0.56 (9:1 CH_2Cl_2-MeOH); ^{1}H NMR (400 MHz, DMSO-d_6): δ (ppm) 13.21 (1 H, br. s, CO_2H), 10.39 (1 H, s, NHCO), 8.01 (2 H, d, J = 8.4, benzoate C-3), 7.94−7.86 (6 H, m, benzoate C-2, ArH-3 and ArH-5, phenyl H-ortho), 7.75 (1 H, app. t, J = 8.0, ArH-4), 7.59−7.51 (3 H, m, phenyl H-meta and phenyl H-para); ^{13}C NMR (100 MHz, $CDCl_3$): δ (ppm) 166.7 (C-5), 165.2 (CO_2H), 161.7 (CO_2NH), 157.8 (C-3), 137.1 (benzoate C-4), 135.3 (PhC-quart), 133.8 (benzoate C-1), 133.6 (ArC-3), 132.2 (ArC-2), 130.9 (q, J = 30.9, ArC-6), 130.6 (benzoate C-4), 129.3 (benzoate C-2), 129.2 (PhC-ortho), 127.9 (PhC-meta), 126.4 (PhC-para), 125.9 (benzoate C-3), 125.7 (q, J = 5.0, ArC-5), 125.1 (ArC-1), 122.9 (q, J = 274.7, CF_3), 114.5 (C-4); LC−MS (ESI): calcd for $C_{24}H_{15}ClF_3N_2O_4$ $[M + H]^+$: 487.06, observed 487.17, LC R_t: 6.73 min. HRMS (ESI): calcd for $C_{24}H_{15}ClF_3N_2O_4$ $[M + H]^+$: 487.0672, observed: 487.0677.

*4.3.24. 4-[({3-[2-Chloro-6-(trifluoromethyl)phenyl]-5-phenyl-1,2-oxazol-4-yl}amino) methyl] Benzoic Acid (**21**).* Methly-4-formyl benzoate (93.0 mg, 0.570 mmol, 1.0 equiv) and AcOH (0.5 mL) were added to a solution of amine **13** (0.201 g, 0.590 mmol, 1.05 equiv) in MeOH (10.0 mL). The reaction mixture was heated at reflux for 18 h after which time it was cooled to room temperature, and $NaCNBH_3$

DOI: 10.1021/acs.jmedchem.9b01372
J. Med. Chem. 2020, 63, 241−259

(74.0 mg, 1.18 mmol, 2.0 equiv) was added. The reaction mixture was heated at reflux for a further 18 h then concentrated in vacuo, diluted with EtOAc (10 mL), and washed with saturated aqueous $NaHCO_3$ (20 mL), water (20 mL), and brine (20 mL). The combined organic phase was dried ($MgSO_4$), filtered, and concentrated in vacuo. The crude product was purified by flash column chromatography, eluting with 17% EtOAc in *n*-heptane, to furnish the ester (0.120 g, 43%). The intermediate product (0.106 g, 0.220 mmol) was subject to ester hydrolysis according to the General Procedure for ester hydrolysis and purified by trituation with Et_2O to furnish **21** (0.094 g, 98%) as a colorless solid. R_f = baseline (1:1 cyclo-hexane-EtOAc); ^{1}H NMR (400 MHz, DMSO-d_6): δ (ppm) 12.82 (1 H, br. s, CO_2H), 7.95 (1 H, d, J = 8.1, ArH-3), 7.88 (1 H, d, J = 8.1, ArH-5), 7.84 (2 H, d, J = 7.3, PhH-ortho), 7.80−7.78 (1 H, m, ArH-4), 7.75 (2 H, d, J = 8.1, benzoate H-2), 7.53−7.50 (2 H, m, PhH-meta), 7.47−7.43 (1 H, m, PhH-para), 7.15 (2 H, d, J = 8.1, benzoate H-3), 5.11 (1 H, app. t, J = 6.0, NHCH$_2$), 4.00 (1 H, dd, J = 15.5, 6.0, NHCH_a), 3.94 (1 H, dd, J = 15.5, 6.0, NHCH_b); ^{13}C NMR (100 MHz, DMSO-d6): δ (ppm) 167.2 (C-5), 155.3 (CO_2H), 154.3 (C-3), 145.0 (benzoate C-4), 136.0 (ArC-2), 133.6 (ArC-3), 132.2 (PhC-quart.), 131.1 (q, J = 30.5, ArC-6), 129.22 (benzoate C-1), 129.17 (ArC-4), 129.0 (PhC-ortho), 128.9 (benzoate C-2), 127.6 (PhC-para), 127.1 (PhC-meta), 126.0 (ArC-5), 125.9 (C-4), 125.7 (benzoate C-3), 125.4 (q, J = 5.0, ArC-1), 122.9 (q, J = 274.6, CF_3), 49.8 (CH_2NH); LC−MS (ESI): calcd for $C_{24}H_{17}ClF_3N_2O_3$ [M + H]$^+$: 473.08, observed 473.17, LC R_t: 7.48 min. HRMS (ESI): calcd for $C_{24}H_{17}ClF_3N_2O_3$ [M + H]$^+$: 473.0880, observed: 473.0883.

*4.3.25. 4-({3-[2-Chloro-6-(trifluoromethyl)phenyl]-5-phenyl-1,2-oxazol-4-yl}sulfamoyl) Benzoic Acid (**22**).* Methyl-4-(chlorosulfonyl)benzoate (0.464 g, 1.70 mmol, 3.0 equiv) was added to a solution of amine **13** (0.192 g, 0.570 mmol, 1.0 equiv) in pyridine (10.0 mL). The reaction mixture was stirred at 60 °C for 24 h then cooled to room temperature and concentrated in vacuo. The mixture was suspended in EtOAc (20 mL) and washed with 1 M aqueous HCl (20 mL), saturated aqueous $NaHCO_3$ (20 mL), water (20 mL), and brine (20 mL). The organic phase was dried ($MgSO_4$), filtered, and concentrated in vacuo to furnish the ester (0.260 g, 71%) that was used without further purification. The intermediate product (0.188 g, 0.350 mmol) was subject to ester hydrolysis according to the General Procedure for ester hydrolysis and purified by trituation with Et_2O to furnish **22** (0.079 g, 43%) as a yellow solid. R_f = baseline (1:1 cyclo-hexane-EtOAc); ^{1}H NMR (400 MHz, DMSO-d_6): δ (ppm) 13.30 (1 H, br. s, CO_2H), 10.49 (1 H, br. s, NHSO$_2$), 7.87 (1 H, d, J = 8.0, ArC-3), 7.79 (1 H, d, J = 8.0, ArC-5), 7.75−7.68 (5 H, m, ArH-4, PhH-ortho, benzoate H-3), 7.51 (2 H, d, J = 8.2, benzoate H-2), 7.46−7.37 (3 H, m, PhH-meta and PhH-para); ^{13}C NMR (100 MHz, DMSO-d6): δ (ppm) 165.9 (C-5), 164.8 (CO_2H), 159.2 (C-3), 143.6 (benzoate C-4), 135.4 (ArC-2), 134.2 (ArC-3), 133.5 (benzoate C-1), 132.3 (PhC-quart.), 130.9 (q, J = 30.9, ArC-6), 130.8 (ArC-4), 129.7 (benzoate C-2), 128.8 (PhC-ortho), 126.2 (benzoate C-3), 126.1 (PhC-meta), 125.5 (q, J = 5.0, ArC-1), 125.2 (PhC-para), 124.4 (ArC-5), 122.8 (q, J = 274.5, CF_3), 112.4 (C-4); LC−MS (ESI): calcd for $C_{23}H_{15}ClF_3N_2O_5S$ [M + H]$^+$: 523.03, observed: 523.00, LC R_t: 6.70 min. HRMS (ESI): calcd for $C_{23}H_{15}ClF_3N_2O_5S$ [M + H]$^+$: 523.0342, observed: 523.0333.

*4.3.26. 4-[({3-[2-Chloro-6-(trifluoromethyl)phenyl]-5-(furan-2-yl)-1,2-oxazol-4-yl}methyl)amino]benzoic Acid (**23**).* According to the General Procedure for reductive amination, aldehyde **39** (0.180 g, 0.520 mmol) was reacted with *tert*-butyl-4-amino benzoate (0.102 g, 0.520 mmol) in MeOH. The crude product was purified by column chromatography, eluting with a gradient of 5−20% EtOAc in *n*-heptane, to furnish the intermediate imine (0.136 g) that was immediately subjected to the reduction step performed in EtOH at 85 °C. The crude product was purified by column chromatography, eluting with a gradient of 10−20% EtOAc in *n*-heptane, to furnish the intermediate amine (0.065 g, 24%). This product was subject to *tert*-butyl ester deprotection according to the General Procedure for *tert*-butyl ester deprotection. The crude product was purified by column chromatography, eluting with 1% MeOH in CH_2Cl_2, to furnish the carboxylic acid **23** (0.040 g, 73%) as a colorless solid. R_f = 0.13 (99:1 CH_2Cl_2-MeOH); ^{1}H NMR (400 MHz, MeOD): δ (ppm) 7.84 (1 H, d, J = 1.8, furanyl H-5), 7.75 (1 H, d, J = 8.1, Ar H-3 or ArH-5), 7.74 (1 H, d, J = 8.1, ArH-3 or ArH-5), 7.61 (1 H, app. t, J = 8.1, ArH-4), 7.61 (2 H, d, J = 8.8, benzoate H-2), 7.12 (1 H, d, J = 3.5, furanyl H-3), 7.62 (1 H, dd, J = 3.5, 1.8, furanyl H-4), 6.34 (2 H, d, J = 8.8, benzoate H-3), 4.46 (1 H, d, J = 15.3, CH_aNH), 4.36 (1 H, d, J = 15.3, CH_bNH); ^{13}C NMR (100 MHz, $CDCl_3$): δ (ppm) 170.5 (C-5), 160.6 (CO_2H), 159.9 (C-3), 153.4 (furanyl C-2), 146.5 (furanyl C-5), 144.1 (benzoate C-4), 137.6 (ArC-2), 134.6 (ArC-3), 132.9 (q, J = 32.5, ArC-6), 132.7 (ArC-4), 132.4 (benzoate C-2), 127.3 (ArC-1), 126.3 (q, J = 5.1, ArC-5), 124.4 (q, J = 273.8, CF_3), 118.7 (benzoate C-1), 114.6 (C-4), 113.2 (furanyl C-4), 113.1 (furanyl C-3), 111.8 (benzoate C-3), 36.4 (CH_2NH); LC−MS (ESI): calcd for $C_{22}H_{15}ClF_3N_2O_4$ [M + H]$^+$: 463.06, observed: 462.92, LC R_t: 6.67 min; HRMS (ESI): calcd for $C_{22}H_{15}ClF_3N_2O_4$ [M + H]$^+$: 463.0672, observed: 463.0661.

*4.3.27. 4-[({3-[2-Chloro-6-(trifluoromethyl)phenyl]-5-(thiophen-2-yl)-1,2-oxazol-4-yl}methyl)amino]benzoic Acid (**24**).* According to the General Procedure for reductive amination, aldehyde **40** (0.096 g, 0.270 mmol) was reacted with *tert*-butyl-4-amino benzoate (0.052 g, 0.27 mmol) in MeOH. The crude product was purified by column chromatography, eluting with a gradient of 5−10% EtOAc in *n*-heptane, to furnish the intermediate imine (0.125 g) that was immediately subjected to the reduction step performed in EtOH at 85 °C for 5 h. The crude product was purified by column chromatography, eluting with a gradient of 3−10% EtOAc in *n*-heptane, to furnish the intermediate amine (24.0 mg, 17%). This product was subject to *tert*-butyl ester deprotection according to the General Procedure for *tert*-butyl ester deprotection. The crude product was purified by column chromatography, eluting with 3% MeOH in CH_2Cl_2, to furnish the carboxylic acid **24** (12.0 mg, 56%) as a pale yellow solid. R_f = 0.13 (98:2 CH_2Cl_2-MeOH); ^{1}H NMR (400 MHz, DMSO-d_6): δ (ppm) 12.02 (1 H, br. s, CO_2H), 7.96 (1 H, dd, J = 5.1, 1.1, thiophenyl H-5), 7.93 (1 H, d, J = 8.0, ArH-3 or ArH-5), 7.87 (1 H, d, J = 8.0, ArH-3 or ArH-5), 7.77−7.73 (2 H, m, ArH-4, thiophenyl H-3), 7.55 (2 H, d, J = 8.8, benzoate H-2), 7.33 (1 H, dd, J = 5.1, 3.7, thiophenyl H-4), 6.48 (1 H, app. t, J = 5.0, CH$_2$NH), 6.42 (2 H, d, J = 8.8, benzoate H-3), 4.20 (1 H, dd, J = 14.8, 5.0, CH_aNH), 4.13 (1 H, dd, J = 14.8, 5.0, CH_bNH); ^{13}C NMR (100 MHz, DMSO-d_6): δ (ppm) 167.4 (C-5), 162.0 (CO_2H), 159.5 (C-3), 151.6 (benzoate C-4), 135.5 (ArC-2), 133.8 (ArC-3), 132.3 (ArC-4), 130.8 (benzoate C-2), 130.6 (q, J = 30.7, ArC-6), 130.6 (thiophenyl C-5), 128.8 (thiophenyl C-3), 128.7 (thiophenyl C-4), 127.2 (thiophenyl C-2), 125.5 (q, J = 4.9, ArC-5), 125.3 (ArC-1), 122.8 (q, J = 274.5, CF_3), 117.6 (benzoate C-1), 112.0 (C-4), 110.8 (benzoate (C-3), 35.6 (CH_2NH); LC−MS (ESI): calcd for $C_{22}H_{15}ClF_3N_2O_3S$ [M + H]$^+$: 479.04, observed: 479.00, LC R_t: 7.23 min. HRMS (ESI): calcd for $C_{22}H_{15}ClF_3N_2O_3S$ [M + H]$^+$: 479.0444, observed: 479.0429.

*4.3.28. 4-[({3-[2-Chloro-6-(trifluoromethyl)phenyl]-5-(1H-pyrrol-3-yl)-1,2-oxazol-4-yl}methyl)amino]benzoic Acid (**25**).* According to the General Procedure for reductive amination, aldehyde **41** (0.060 g, 0.176 mmol) was reacted with methyl-4-amino benzoate (0.032 g, 0.211 mmol) in MeOH. The crude product was purified by column chromatography, eluting with 25% EtOAc in *n*-heptane, to furnish the intermediate imine (0.034 mg) that was immediately subjected to the reduction step performed in MeOH at reflux for 2 h. The crude product was purified by column chromatography, eluting with a gradient of 20% EtOAc in *n*-heptane, to furnish the intermediate amine (16.3 mg, 19%). This product was subject to ester hydrolysis according to the General Procedure for *tert*-Butyl ester deprotection. The crude product was purified by column chromatography, eluting with 1.5% MeOH in CH_2Cl_2, to furnish the carboxylic acid **25** (5.40 mg, 57%) as a colorless solid. R_f = 0.10 (96:4 CH_2Cl_2-MeOH); ^{1}H NMR (400 MHz, DMSO-d_6): δ (ppm) 11.99 (1 H, br. s, CO_2H), 11.52 (1 H, s, pyrrole-NH), 7.91 (1 H, d, J = 8.1, ArH-3 or ArH-5), 7.85 (1 H, d, J = 7.9, ArH-3 or ArH-5), 7.72 (1 H, app. t, J = 8.0, ArH-4), 7.54 (2 H, d, J = 8.4, benzoate C-2), 7.39 (1 H, m, pyrrole H-2), 6.98 (1 H, app. q, J = 2.4, pyrrole H-5), 6.55 (1 H, d, J = 2.4, pyrrole H-4), 6.42 (2 H, d, J = 8.4, benzoate H-3), 6.34 (1 H, app. t, J = 5.0,

DOI: 10.1021/acs.jmedchem.9b01372
J. Med. Chem. 2020, 63, 241−259

CH_2NH), 4.08 (1 H, dd, J = 14.5, 5.0, CH_aNH), 4.00 (1 H, dd, J = 14.5, 5.0, CH_aNH); ^{13}C NMR (100 MHz, DMSO-d_6): δ (ppm) 167.9 (C-5), 165.7 (CO_2H), 159.2 (C-3), 152.3 (benzoate C-4), 136.0 (ArC-2), 134.1 (ArC-3), 132.4 (ArC-4), 131.3 (benzoate C-2), 130.9 (q, J = 30.4, ArC-6), 126.8 (ArC-1), 125.8 (q, J = 5.0, ArC-5), 122.0 (q, J = 274.3, CF_3), 120.5 (pyrrole C-5), 119.2 (pyrrole C-2), 117.8 (benzoate C-1), 111.2 (benzoate C-3), 110.5 (C-4), 109.2 (pyrrole C-3), 106.7 (pyrrole C-4), 36.2 (CH_2NH); LC−MS (ESI): calcd for $C_{22}H_{16}ClF_3N_3O_3$ $[M + H]^+$: 462.08, observed: 462.00, LC R_t: 6.20 min. HRMS (ESI): calcd for $C_{22}H_{16}ClF_3N_3O_3$ $[M + H]^+$: 462.0832, observed: 462.0834.

*4.3.29. 4-[({3-[2-Chloro-6-(trifluoromethyl)phenyl]-5-(naphthalen-1-yl)-1,2-oxazol-4-yl}methyl)amino]benzoic Acid (**26**).* According to the General Procedure for reductive amination, aldehyde **42** (0.034 g, 0.0850 mmol) was reacted with *tert*-butyl-4-amino benzoate (0.016 g, 0.085 mmol) in MeOH. The crude product was purified by column chromatography, eluting with a gradient of 2−10% EtOAc in *n*-heptane, to furnish the intermediate imine (0.010 g) that was immediately subjected to the reduction step performed in EtOH at 85 °C for 5 h. The crude product was purified by column chromatography, eluting with 20% EtOAc in *n*-heptane, to furnish the intermediate amine (8.00 mg, 16%). This product was subjected to *tert*-butyl ester deprotection according to the General Procedure for *tert*-Butyl ester deprotection. The crude product was purified by column chromatography, eluting with 3% MeOH in CH_2Cl_2, to furnish the carboxylic acid **26** (3.00 mg, 48%) as a colorless solid. R_f = 0.16 (96:4 CH_2Cl_2-MeOH); ^{1}H NMR (400 MHz, DMSO-d_6): δ (ppm) 11.93 (1 H, br. s, CO_2H), 8.23 (1 H, d, J = 8.3, naphthyl-H), 8.12 (1 H, d, J = 7.5, naphthyl-H), 7.94 (1 H, d, J = 8.0, ArH-3 or ArH-5), 7.88 (1 H, d, J = 8.0, ArH-3 or ArH-5), 7.84 (1 H, d, J = 7.0, naphthyl-H), 7.76−7.66 (5 H, m, ArH-4, naphthyl-H), 7.31 (2 H, d, J = 8.3, benzoate C-2), 6.36 (1 H, app. t, J = 5.8, CH_2NH), 6.08 (2 H, d, J = 8.3, benzoate C-3), 4.08 (1 H, dd, J = 15.8, 5.8, CH_aNH), 4.01 (1 H, dd, J = 15.8, 5.8, CH_aNH); ^{13}C NMR (100 MHz, DMSO-d_6): δ (ppm) 167.3 (C-5), 166.9 (CO_2H), 158.8 (C-3), 151.3 (benzoate C-4), 135.4 (ArC-2), 133.7 (ArC-3), 133.3 (naphthyl-C), 132.1 (ArC-4), 131.4 (naphthyl-C), 130.9 (naphthyl-C), 130.5 (q, J = 31.1, ArC-6), 130.5 (benzoate C-2), 129.3 (naphthyl-C), 128.7 (naphthyl-C), 127.8 (naphthyl-C), 126.8 (naphthyl-C), 125.8 (ArC-1), 125.5 (q, J = 4.0, ArC-5), 125.4 (naphthyl-C), 124.3 (naphthyl-C), 123.5 (naphthyl-C), 123.0 (q, J = 274.3, CF_3), 117.2 (benzoate C-1), 116.3 (C-4), 110.4 (benzoate C-3), 35.3 (CH_2NH); LC−MS (ESI): calcd for $C_{28}H_{19}ClF_3N_2O_3$ $[M + H]^+$: 523.10, observed: 522.92, LC R_t: 7.68 min. HRMS (ESI): calcd for $C_{28}H_{19}ClF_3N_2O_3$ $[M + H]^+$: 523.1036, observed: 523.1046.

*4.3.30. 4-[({3-[2-Chloro-6-(trifluoromethyl)phenyl]-5-(3-hydroxyphenyl)-1,2-oxazol-4-yl}methyl)amino]benzoic Acid (**27**).* According to the General Procedure for reductive amination, aldehyde **43** (0.123 g, 0.255 mmol) was reacted with methyl-4-amino benzoate (0.038 g, 0.255 mmol) in MeOH. The crude product was purified by column chromatography, eluting with a gradient of 2−12% EtOAc in *n*-heptane, to furnish the intermediate imine (0.053 g) that was immediately subjected to the reduction step performed in MeOH at reflux for 3.5 h. This step occurred with concomitant loss of the silyl protecting group. The crude product was purified by column chromatography, eluting with a gradient of 15−35% EtOAc in *n*-heptane, to furnish the intermediate amine (21.0 mg, 16%). This product was subject to ester hydrolysis according to the General Procedure for *tert*-butyl ester deprotection. The crude product was purified by column chromatography, eluting with 3% MeOH in CH_2Cl_2, to furnish the carboxylic acid **27** (17.4 mg, 99%) as a colorless solid. R_f = 0.10 (96:4 CH_2Cl_2-MeOH); ^{1}H NMR (400 MHz, DMSO-d_6): δ (ppm) 7.90 (1 H, d, J = 8.1, ArH-3 or ArH-5), 7.85 (1 H, d, J = 8.0, ArH-3 or ArH-5), 7.72 (1 H, app. t, J = 8.0, ArH-4), 7.52 (2 H, d, J = 8.8, benzoate H-2), 7.40 (1 H, app. t, J = 8.0, phenol H-5), 1.30−7.26 (2 H, m, phenol H-2 and phenol H-4), 6.99 (1 H, dd, J = 8.0, 1.5, phenol H-6), 6.42 (1 H, t, J = 5.0, CH_2NH), 6.36 (2 H, d, J = 8.8, benzoate H-3), 4.17 (1 H, dd, J = 14.6, 5.0, CH_aNH), 4.09 (1 H, dd, J = 14.6, 5.0, CH_bNH); ^{13}C NMR (100 MHz, DMSO-d_6): δ (ppm) 167.4 (C-5), 166.4 (CO_2H), 159.6 (C-3), 157.9 (phenol C-3), 151.6 (benzoate C-4), 135.5 (ArC-2), 133.7 (ArC-3), 132.2 (ArC-4), 130.8 (benzoate C-2), 130.5 (q, J = 30.7, ArC-6), 130.5 (phenol C-1), 127.7 (phenol C-5), 125.7 (ArC-1), 125.4 (q, J = 4.0, ArC-5), 122.8 (q, J = 274.3, CF_3), 117.8 (phenol C-6), 117.6 (benzoate C-1), 113.6 (phenol C-2), 112.9 (C-4), 110.7 (benzoate C-3), 35.7 (CH_2NH); LC−MS (ESI): calcd for $C_{24}H_{17}ClF_3N_2O_4$ $[M + H]^+$: 489.08, observed: 489.00, LC R_t: 6.30 min. HRMS (ESI): calcd for $C_{24}H_{17}ClF_3N_2O_4$ $[M + H]^+$: 489.0829, observed: 489.0823.

*4.3.31. Methyl 5-Bromo-3-[2-chloro-6-(trifluoromethyl)phenyl]-1,2-oxazole-4-carboxylate (**30a**).* Methyl 3-bromopropiolate (prepared according to ref 44, 2.04 g, 12.5 mmol, 1.0 equiv) was added to a solution of nitrile oxide **33** (2.75 g, 12.5 mmol, 1.0 equiv) in THF (25.0 mL), and the reaction mixture was heated at reflux for 4 h. The reaction mixture was concentrated in vacuo to give a crude product as a 7:3 mixture of regioisomers. Purification by recrystallization from hot *n*-heptane furnished bromide **30a** (2.05 g, 43%) as a colorless solid (97:3 mixture of regioisomers, see Supporting Information). R_f = 0.20 (7:3 *n*-heptane-EtOAc); ^{1}H NMR (400 MHz, $CDCl_3$): δ (ppm) 7.73 (1 H, d, J = 8.6, ArH-3 or ArH-5), 7.71 (1 H, d, J = 8.9, ArH-3 or ArH-5), 7.58 (1 H, app. t. J = 8.0, ArH-3), 3.70 (3 H, s, CO_2CH_3); ^{13}C NMR (100 MHz, $CDCl_3$): δ (ppm) 160.0 (C-5), 159.7 (CO_2Me), 148.0 (C-3), 136.3 (ArC-2), 133.0 (ArC-3), 131.7 (q, J = 31.7, ArC-6), 131.3 (ArC-4), 126.0 (ArC-1), 124.8 (q, J = 5.0, ArC-5), 122.9 (q, J = 274.4, CF_3), 113.2 (C-4), 52.3 (CO_2CH_3); LC−MS (ESI): calcd for $C_{12}H_7BrClF_3NO_3$ $[M + H]^+$: 383.92, observed 386.00, LC R_t: 7.12 min.

*4.3.32. [2-Chloro-6-(trifluoromethyl)phenyl]formonitrile Oxide (**33**).* NEt_3 (5.80 mL, 41.5 mmol, 1.2 equiv) was added dropwise to a solution of imidoyl chloride **9a** (8.90 g, 34.6 mmol, 1.0 equiv) in THF (110 mL). A white precipitate formed immediately. The resulting suspension was stirred vigorously at room temperature for 30 min and then filtered through a pad of SiO_2 that was subsequently washed with THF (250 mL). The solution was concentrated in vacuo to furnish **33** (8.25 g, 99%) as a colorless solid which was used immediately. R_f = 0.33 (9:1 c-hexane-EtOAc); ^{1}H NMR (400 MHz, $CDCl_3$): δ (ppm) 7.70 (1 H, d, J = 8.2, H-3 or H-5), 7.67 (1 H, d, J = 8.2, H-3 or H-5), 7.54 (1 H, app. t, J = 8.2, H-4).

*4.3.33. Methyl 3-[2-Chloro-6-(trifluoromethyl)phenyl]-5-(furan-2-yl)-1,2-oxazole-4-carboxylate (**34**).* According to the General Procedure for Suzuki coupling, bromide **30a** (0.150 g, 0.390 mmol) was coupled to furan-2-boronic acid pinacol ester (0.114 g, 0.585 mmol). The crude product was purified by flash column chromatography, eluting with a gradient of 10−50% EtOAc in *n*-heptane, to furnish **34** (0.088 g, 58%) as a colorless solid. R_f = 0.19 (85:15 *n*-heptane-EtOAc); ^{1}H NMR (400 MHz, $CDCl_3$): δ (ppm) 7.82 (1 H, dd, J = 3.6, 0.7, furanyl H-5), 7.73 (1 H, d, J = 8.0, Ar H-3 or ArH-5), 7.72 (1 H, dd, J = 1.8, 0.7, furanyl H-3), 7.70 (1 H, d, J = 8.0, Ar H-3 or ArH-5), 7.56 (1 H, app. t, J = 8.0, ArH-4), 6.66 (1 H, dd, J = 3.6, 1.8, furanyl H-4), 3.62 (3 H, s, CO_2CH_3); ^{13}C NMR (100 MHz, $CDCl_3$): δ (ppm) 163.4 (C-5), 160.9 (CO_2CH_3), 158.7 (C-3), 146.3 (furanyl C-3), 141.6 (furanyl C-2), 136.3 (ArC-2), 132.8 (ArC-3 and ArC-4), 131.6 (q, J = 31.3, ArC-6), 130.8 (ArC-4), 127.1 (ArC-1), 124.7 (q, J = 5.0, ArC-5), 123.0 (q, J = 274.5, CF_3), 118.3 (furanyl C-5), 112.6 (furanyl C-4), 107.3 (C-4), 51.9 (CO_2CH_3); LC−MS (ESI): calcd for $C_{16}H_{10}ClF_3NO_4$ $[M + H]^+$: 371.02, observed: 372.08, LC R_t: 7.77 min.

*4.3.34. Methyl 3-[2-Chloro-6-(trifluoromethyl)phenyl]-5-(thiophen-2-yl)-1,2-oxazole-4-carboxylate (**35**).* According to the General Procedure for Suzuki coupling, bromide **30a** (0.250 g, 0.650 mmol) was coupled to thiophene-2-boronic acid pinacol ester (0.273 g, 1.30 mmol). The crude product was purified by flash column chromatography, eluting with a gradient of 5−20% EtOAc in *n*-heptane, to furnish **35** (0.136 g, 54%) as a colorless solid. R_f = 0.32 (4:1 *n*-heptane-EtOAc); ^{1}H NMR (400 MHz, $CDCl_3$): δ (ppm) 8.29 (1 H, dd, J = 3.9, 1.2, thiophenyl H-5), 7.75−7.69 (3 H, m, ArH-3, ArH-5, thiophenyl H-3), 7.57 (1 H, app. t, J = 8.0, ArH-4), 7.24 (1 H, dd, J = 5.1, 3.9, thiophenyl H-4), 3.64 (3 H, s, CO_2CH_3); ^{13}C NMR (100 MHz, $CDCl_3$): δ (ppm) 167.9 (C-5), 161.4 (CO_2CH_3), 159.2 (C-3), 136.3 (ArC-2), 132.8 (thiophenyl C-5), 132.7 (ArC-4), 132.2 (ArC-3 and thiophenyl C-3), 131.7 (q, J = 31.4, ArC-6), 130.8 (ArH-

DOI: 10.1021/acs.jmedchem.9b01372
J. Med. Chem. 2020, 63, 241−259

4), 128.0 (thiophenyl C-4), 127.4 (thiophenyl C-2), 127.3 (ArC-1), 124.7 (q, J = 5.0, ArC-5), 123.0 (q, J = 274.5, CF_3), 107.2 (C-4), 51.9 (CO_2CH_3); LC−MS (ESI): calcd for $C_{16}H_{10}ClF_3NO_3S$ $[M + H]^+$: 387.99, observed: 388.25, LC R_t: 7.62 min.

*4.3.35. Methyl 5-{1-[(tert-Butoxy)carbonyl]-1H-pyrrol-3-yl}-3-[2-chloro-6-(trifluoromethyl)phenyl]-1,2-oxazole-4-carboxylate (**36**).* According to the General Procedure for Suzuki coupling, bromide **30a** (0.250 g, 0.650 mmol) was coupled to *tert*-butyl 3-(4,4,5,5-tetramethyl-1,3,2-dioxaborolan-2-yl)-1H-pyrrole-1-carboxylate (0.381 g, 1.30 mmol). The crude product was purified by flash column chromatography, eluting with a gradient of 5−20% EtOAc in *n*-heptane, to furnish **36** (0.119 g, 39%) as a colorless oil. R_f = 0.30 (4:1 *n*-heptane-EtOAc); ^{1}H NMR (400 MHz, $CDCl_3$): δ (ppm) 8.45 (1 H, app. t, J = 2.0, pyrrole H-2), 7.72−7.67 (2 H, m, ArH-3 and ArH-5), 7.54 (1 H, app. t, J = 7.9, ArH-4), 7.35 (1 H, dd, J = 3.4, 2.0, pyrrole H-5), 6.98 (dd, J = 3.4, 2.0, pyrrole H-4), 3.61 (3 H, s, CO_2CH_3), 1.63 (9 H, s, $C(CH_3)_3$); ^{13}C NMR (100 MHz, $CDCl_3$): δ (ppm) 168.9 (C-5), 161.6 (CO_2CH_3), 159.0 (C-3), 148.2 (NCO_2), 136.3 (ArC-2), 132.8 (ArC-3), 131.6 (q, J = 31.3, ArC-6), 130.6 (ArC-4), 127.7 (ArC-1), 124.7 (q, J = 5.0, ArC-5), 124.1 (pyrrole C-2), 123.0 (q, J = 274.4, CF_3), 121.0 (pyrrole C-5), 113.8 (pyrrole C-3), 111.5 (pyrrole C-4), 107.2 (C-4), 85.2 ($C(CH_3)_3$), 51.7 (CO_2CH_3), 28.0 ($C(CH_3)_3$); LC−MS (ESI): calcd for $C_{21}H_{19}ClF_3N_2O_5$ $[M + H]^+$: 471.09, observed: 471.17, LC R_t: 8.55 min.

*4.3.36. Methyl 3-[2-Chloro-6-(trifluoromethyl)phenyl]-5-(naphthalen-1-yl)-1,2-oxazole-4-carboxylate (**37**).* According to the General Procedure for Suzuki coupling, bromide **30a** (0.150 g, 0.390 mmol) was coupled to naphthalene-1-boronic acid pinacol ester (0.198 g, 0.780 mmol). The crude product was purified by flash column chromatography, eluting with a gradient of 10− 20% EtOAc in *n*-heptane, to furnish **37** (0.059 g, 35%) as a colorless oil. R_f = 0.43 (4:1 *n*-heptane-EtOAc); ^{1}H NMR (400 MHz, $CDCl_3$): δ (ppm) 8.07 (1 H, d, J = 8.3, naphthyl-H), 7.97−7.94 (1 H, m, naphthyl-H), 7.81−7.75 (3 H, m, naphthyl-H), 7.73−7.71 (1 H, m, ArH-3 or ArH-5), 7.65−7.60 (2 H, m, ArH-3 or ArH-5, naphthyl-H), 7.58−7.56 (2 H, m, ArH-3 or ArH-5, naphthyl-H), 3.41 (3 H, s, CO_2CH_3); ^{13}C NMR (100 MHz, $CDCl_3$): δ (ppm) 173.7 (C-5), 161.0 (CO_2CH_3), 158.9 (C-4), 136.4, 133.5, 132.9, 131.9, 131.8 (q, J = 31.4, ArC-6), 131.4, 130.9, 130.2, 129.4, 128.7, 127.6, 127.1 (ArC-1), 126.7, 124.9, 124.8, 124.2, 123.2 (q, J = 274.4, CF_3), 112.2 (C-4), 51.8 (CO_2CH_3), (not all peaks could be precisely assigned with certainty); LC−MS (ESI): calcd for $C_{22}H_{14}ClF_3NO_3$ $[M + H]^+$: 432.05, observed: 432.25, LC R_t: 8.14 min.

*4.3.37. Methyl 5-{3-[(tert-Butyldimethylsilyl)oxy]phenyl}-3-[2-chloro-6-(trifluoromethyl)phenyl]-1,2-oxazole-4-carboxylate (**38**).* According to the General Procedure for Suzuki coupling, bromide **30a** (0.400 g, 1.04 mmol) was coupled to 3-(4,4,5,5-tetramethyl-1,3,2-dioxaborolan-2-yl)phenol (0.319 g, 1.45 mmol). The crude product was purified by flash column chromatography, eluting with a gradient of 10−20% EtOAc in *n*-heptane, to furnish the phenol (0.167 g, 40%) as a colorless solid. Imidazole (94.0 mg, 1.38 mmol, 3.0 equiv) and *tert*-butyldimethylsilyl chloride (0.104 g, 0.690 mmol, 1.5 equiv) were added to a solution of the phenol (0.183 g, 0.460 mmol, 1.0 equiv) in DMF (3.0 mL). The reaction mixture was stirred at room temperature for 3 h then diluted with saturated aqueous NH_4Cl (20 mL) and extracted with EtOAc (2 × 20 mL). The combined organic phase was washed with water (2 × 50 mL) and brine (50 mL), dried ($MgSO_4$), filtered, and concentrated in vacuo. The crude product was purified by column chromatography, eluting with a gradient of 0−20% EtOAc in *n*-heptane, to furnish silyl ether **38** (56.0 mg, 70%) as a colorless oil. R_f = 0.26 (9:1 *n*-heptane-EtOAc); ^{1}H NMR (400 MHz, $CDCl_3$): δ (ppm) 7.73 (2 H, app. t, J = 8.6, ArH-3 and ArH-5), 7.70 (1 H, ddd, J = 8.1, 1.7, 1.0, phenol H-4), 7.59−7.55 (2 H, m, phenol H-2, ArH-4), 7.39 (1 H, app. t, J = 8.1, phenol H-5), 7.04 (1 H, ddd, J = 8.1, 2.4, 1.0, phenol H-6), 3.59 (3 H, s, CO_2CH_3), 1.02 (9 H, s, $Si(CH_3)_2C(CH_3)_3$), 0.26 (6 H, s, $Si(CH_3)_2C(CH_3)_3$); ^{13}C NMR (100 MHz, $CDCl_3$): δ (ppm) 172.7 (C-5), 161.4 (CO_2CH_3), 159.4 (C-3), 155.9 (phenol C-3), 136.4 9ArC-2), 132.9 (ArC-3), 131.7 (q, J = 31.3, ArC-6), 130.8 (ArC-4), 129.7 (phenol C-5), 127.6 (ArC-1), 127.5 (phenol C-1), 124.8 (q, J = 5.0, ArC-5), 123.7 (phenol C-6), 123.0 (q, J = 274.4, CF_3), 122.4 (phenol C-4), 120.8 (phenol C-2), 109.3 (C-4), 52.0 (CO_2CH_3), 25.8 ($Si(CH_3)_2C(CH_3)_3$), 18.3 ($Si(CH_3)_2C(CH_3)_3$), −4.3 ($Si(CH_3)_2C(CH_3)_3$); LC−MS (ESI): calcd for $C_{24}H_{26}ClF_3NO_4Si$ $[M + H]^+$: 512.12, observed: 512.25, LC R_t: 9.62 min.

*4.3.38. 3-[2-Chloro-6-(trifluoromethyl)phenyl]-5-(furan-2-yl)-1,2-oxazole-4-carbaldehyde (**39**).* Ester **34** (0.192 g, 0.516 mmol) was treated according to the General Procedure for conversion of esters to aldehydes, to furnish aldehyde **39** (0.169 g, 96%) as a colorless oil. The crude product was used without further purification. R_f = 0.51 (3:2 *n*-heptane-EtOAc); ^{1}H NMR (400 MHz, $CDCl_3$): δ (ppm) 10.20 (1 H, s, C*H*O), 7.77 (1 H, dd, J = 1.8, 0.8, furanyl H-5), 7.76 (1 H, d, J = 8.0, Ar H-3 or ArH-5), 7.73 (1 H, d, J = 7.8, ArH-3 or ArH-5), 7.60 (1 H, app. t, J = 8.0, ArH-4), 7.55 (1 H, dd, J = 3.6, 0.8, furanyl H-3), 6.72 (1 H, dd, J = 3.6, 1.8, furanyl H-4); ^{13}C NMR (100 MHz, $CDCl_3$): δ (ppm) 182.8 (*C*HO), 164.1 (C-5), 154.7 (C-3), 147.2 (furanyl C-3), 142.2 (furanyl C-2), 136.2 (ArC-2), 133.1 (ArC-3), 131.8 (q, J = 31.5, ArC-6), 131.3 (ArC-4), 125.6 (ArC-1), 125.0 (q, J = 5.0, ArC-5), 122.9 (q, J = 274.5, CF_3), 116.9 (furanyl C-5), 115.2 (C-4), 112.9 (furanyl C-4); LC−MS (ESI): calcd for $C_{15}H_8ClF_3NO_3$ $[M + H]^+$: 342.01, observed: 342.08, LC R_t: 6.93 min.

*4.3.39. 3-[2-Chloro-6-(trifluoromethyl)phenyl]-5-(thiophen-2-yl)-1,2-oxazole-4-carbaldehyde (**40**).* Ester **35** (0.082 g, 0.210 mmol) was treated according to the General Procedure for conversion of esters to aldehydes. The crude product was purified by flash column chromatography, eluting with a gradient of 2−10% EtOAc in *n*-heptane, to furnish aldehyde **40** (0.048 g, 64%) as a colorless solid. R_f = 0.28 (4:1 *n*-heptane-EtOAc); ^{1}H NMR (400 MHz, $CDCl_3$): δ (ppm) 9.78 (1 H, s, C*H*O), 8.32 (1 H, dd, J = 3.9, 1.2, thiophenyl H-5), 7.80−7.75 (3 H, m, ArH-3, ArH-5, thiophenyl H-3), 7.64 (1 H, app. t, J = 8.1, ArH-4), 7.29 (1 H, dd, J = 5.1, 3.9, thiophenyl H-4); ^{13}C NMR (100 MHz, $CDCl_3$): δ (ppm) 182.2 (*C*HO), 168.0 (C-5), 159.0 (C-3), 136.6 (ArC-2), 133.4 (thiophenyl C-5), 132.9 (ArC-3), 132.8 (ArC-4), 132.3 (q, J = 31.5, ArC-6), 131.6 (thiophenyl C-3), 128.7 thiophenyl C-4), 127.0 (thiophenyl C-2), 125.3 (ArC-1), 125.2 (q, J = 5.0, ArC-5), 122.9 (q, J = 274.5, CF_3), 114.4 (C-4); LC−MS (ESI): calcd for $C_{15}H_8ClF_3NO_2S$ $[M + H]^+$: 357.98, observed: 358.17, LC R_t: 7.27 min.

*4.3.40. 3-[2-Chloro-6-(trifluoromethyl)phenyl]-5-(1H-pyrrol-3-yl)-1,2-oxazole-4-carbaldehyde (**41**).* Ester **36** (0.228 g, 0.486 mmol) was treated according to the General Procedure for conversion of esters to aldehydes with a modification: the reduction step was performed with 3.0 equiv of reducing agent and without cooling; this step occurred with concomitant loss of the Boc protecting group. The crude product was purified by flash column chromatography, eluting with 30% EtOAc in *n*-heptane, to furnish aldehyde **41** (0.084 g, 51%) as a brown solid. R_f = 0.20 (7:3 *n*-heptane-EtOAc); ^{1}H NMR (400 MHz, $CDCl_3$): δ (ppm) 9.62 (1 H, s, C*H*O), 8.77 (1 H, br. s, N*H*), 8.26 (1 H, app. dt, J = 3.3, 1.7, pyrrole H-2), 7.78 (1 H, d, J = 8.0, ArH-3 or ArH-5), 7.75 (1 H, d, J = 8.0, ArH-3 or ArH-5), 7.61 (1 H, app. t, J = 8.0, ArH-4), 7.02−6.95 (1 H, m, pyrrole H-5), 6.95 (1 H, dd, J = 2.7, 1.7, pyrrole H-4); ^{13}C NMR (100 MHz, $CDCl_3$): δ (ppm) 182.8 (*C*HO), 170.7 (C-5), 160.0 (C-3), 133.6 (ArC-2), 133.3 (ArC-3), 132.3 (q, J = 31.5, ArC-6), 131.4 (ArC-4), 125.7 (ArC-1), 125.1 (q, J = 5.0, ArC-5), 123.8 (pyrrole C-2), 122.9 (q, J = 274.5, CF_3), 120.3 (pyrrole C-5), 113.2 (pyrrole C-3), 110.7 (C-4), 108.6 (pyrrole C-4); LC−MS (ESI): calcd for $C_{15}H_9ClF_3N_2O_2$ $[M + H]^+$: 341.02, observed: 341.08, LC R_t: 6.33 min.

*4.3.41. 3-[2-Chloro-6-(trifluoromethyl)phenyl]-5-(naphthalen-1-yl)-1,2-oxazole-4-carbaldehyde (**42**).* Ester **37** (0.068 g, 0.160 mmol) was treated according to the General Procedure for conversion of esters to aldehydes. The crude product was purified by flash column chromatography, eluting with 17% EtOAc in *n*-heptane, to furnish aldehyde **42** (0.039 g, 61%) as a colorless solid. R_f = 0.28 (4:1 *n*-heptane-EtOAc); ^{1}H NMR (400 MHz, $CDCl_3$): δ (ppm) 9.73 (1 H, s, C*H*O), 8.14 (1 H, d, J = 8.5, naphthyl-H), 8.02−7.98 (2 H, m, naphthyl-H), 7.83 (1 H, dd, J = 7.1, 1.2. naphthyl-H), 7.79 (1 H, d, J = 8.0, ArH-3 or ArH-5), 7.76 (1 H, d, J = 8.0, ArH-3 or ArH-5),

DOI: 10.1021/acs.jmedchem.9b01372
J. Med. Chem. 2020, 63, 241−259

7.68−7.61 (4 H, m, ArH-4 and naphthy-H); ^{13}C NMR (100 MHz, $CDCl_3$): δ (ppm) 183.1 (CHO), 176.6 (C-5), 157.4 (C-4), 136.3, 133.8, 133.1, 132.9, 131.8 (q, J = 31.5, ArC-6), 131.4, 131.2, 130.1, 128.9, 128.5, 127.3, 126.1 (ArC-1), 125.1, 125.0 (q, J = 5.0, ArC-5), 124.7, 123.1 (q, J = 274.4, CF_3), 122.5, 118.7 (C-4) (not all peaks could be precisely assigned with certainty); LC−MS (ESI): calcd for $C_{21}H_{12}ClF_3NO_2$ $[M + H]^+$: 402.04, observed: 401.92, LC R_t: 8.15 min.

*4.3.42. 5-{3-[(tert-Butyldimethylsilyl)oxy]phenyl}-3-[2-chloro-6-(trifluoromethyl)phenyl]-1,2-oxazole-4-carbaldehyde (**43**).* Ester **38** (0.173 g, 0.340 mmol) was treated according to the General Procedure for conversion of esters to aldehydes. The crude product was purified by flash column chromatography, eluting with a gradient of 0−10% EtOAc in *n*-heptane, to furnish aldehyde **43** (0.123 g, 80%) as a colorless solid. R_f = 0.34 (9:1 *n*-heptane-EtOAc); ^{1}H NMR (400 MHz, $CDCl_3$): δ (ppm) 9.94 (1 H, s, CHO), 7.77 (1 H, d, J = 8.0, ArH-3 or ArH-5), 7.74 (1 H, d, J = 8.0, ArH-3 or ArH-5), 7.63−7.59 (2 H, m, phenol H-4 and phenol H-5), 7.51 (1 H, app. t, J = 2.0, phenol H-2), 7.46 (1 H, app. t, J = 8.0, ArH-4), 7.11 (1 H, ddd, J = 8.2, 2.0, 1.0, phenol H-6), 1.02 (9 H, s, $Si(CH_3)_2C(CH_3)_3$), 0.27 (6 H, s, $Si(CH_3)_2C(CH_3)_3$); ^{13}C NMR (100 MHz, $CDCl_3$): δ (ppm) 182.8 (CHO), 174.4 (C-5), 158.5 (C-3), 156.6 (phenol C-3), 136.4 (ArC-2), 133.2 (ArC-3), 132.0 (q, J = 31.6, ArC-6), 131.3 (ArC-4), 130.6 (phenol C-5), 126.8 (ArC-1), 126.0 (phenol C-1), 125.0 (q, J = 5.1, ArC-5), 124.6 (phenol C-6), 123.0 (q, J = 274.5, CF_3), 122.0 (phenol C-4), 120.3 (phenol C-2), 116.3 (C-4), 25.6 ($Si(CH_3)_2C(CH_3)_3$), 18.4 ($Si(CH_3)_2C(CH_3)_3$), −4.2 ($Si(CH_3)_2C(CH_3)_3$); LC−MS (ESI): calcd for $C_{23}H_{24}ClF_3NO_3Si$ $[M + H]^+$: 482.11, observed: 482.17, LC R_t: 9.45 min.

4.4. Biophysical Assays. *4.4.1. RORγt-LBD Expression and Purification (Used for TR-FRET Assays).* A pET15b expression vector encoding the human RORγt LBD (residues 265−518) with an *N*-terminal His_6-tag was transformed by heat shock into BL21(DE3) *E. coli* cells. Single colonies were used to inoculate precultures of 8 mL LB-media containing 100 μg/mL ampicillin. After overnight incubation at 37 °C, each preculture was transferred to 1L TB media supplemented with ampicillin (100 μg/mL) and incubated at 37 °C until an $OD_{600\ nm}$ = 1.0 was reached. Protein expression was then induced with 0.5 mM isopropyl-*b*-d-thiogalactoside (IPTG), and cultures were incubated for 16 h at 18°C. The cells were collected by centrifugation and suspended in lysis buffer (300 mM NaCl, 20 mM TrisHCl pH 8.0, 20 mM imidazole, 1 mM TCEP, 10% v/v glycerol, complete, EDTA-free Protease Inhibitor Cocktail tablets (1 tablet/50 mL lysate) and benzonase (0.1 μL/1 mL)). After lysis using a C3 Emulsiflex-C3 homogenizer (Avestin), the cell lysate was cleared by centrifugation at 4 °C and the protein was purified via Ni^{2+} affinity column chromatography. Fractions containing the protein of interest were combined and dialyzed against 150 mM NaCl, 20 mM Tris HCl pH 8.0, 5 mM DTT, and 10% v/v glycerol.

4.4.2. TR-FRET Coactivator Recruitment Assay. Assays were conducted using 100 nM *N*-terminal biotinylated SRC-1 box2 peptide (Biotin-N-PSSHSSLTARHKILHRLLQEGSPSD-$CONH_2$) and 20 nM His_6-RORγt-LBD or 100 nM His_6-PPARγ-LBD in buffer containing 10 mM HEPES, 150 mM NaCl, 5 mM DTT, 0.1% BSA (w/v), and 0.1 mM CHAPS, pH 7.5. A terbium labeled anti-His antibody (CisBio Bioassays, 61HISTLA) and D2-labeled streptavidin (CisBio Bioassays, 610SADLA) were used at the concentrations recommended by the supplier. In the case of PPARγ, the assay was performed in the presence of 1 μM rosiglitazone, in order to initially activate PPARγ. Compounds (dissolved in DMSO) were titrated using a 2× dilution series in Corning white low volume, low binding, 384-well plates at a final volume of 10 μL. The final DMSO concentration was 2% v/v throughout. The plate was incubated at room temperature for 30 min and centrifuged before reading (excitation = 340 nm; emission = 665 and 620 nm) on a Tecan infinite F500 plate reader using the parameters recommended by CisBio Bioassays. The data were analyzed with Origin Software. The dose−response curve was fitted represented by

$$y = A_1 + \frac{A_1 - A_2}{1 + 10^{(\log(x_0) - x)p}}$$

where y is the FRET ratio, A_1 is the bottom asymptote, A_2 is the top asymptote, p is the Hills slope, and x is the ligand concentration. Where dose−response curves did not reach a bottom asymptote, this was fixed at the value of the negative control. (Data recorded in triplicate; error shown is standard deviation from the mean; curves are representative of >3 repeated experiments).

4.4.3. Competition TR-FRET Coactivator Recruitment Assay. Competition assays were performed in an analogous fashion to that described above only in the presence of fixed concentrations of cholesterol: 0 μM (DMSO), 0.25 μM, 1.0 μM, such that the final concentration of DMSO remained at 1.2% v/v.

4.4.4. Ligand Binding TR-FRET Assay. Assays were conducted using 100 nM Alexa647-labeled MRL-871 and 20 nM His_6-RORγt-LBD in buffer as described above. A terbium-labeled anti-His antibody (CisBio Bioassays, 61HISTLA) was used at the concentrations recommended by the supplier. The assay was carried out in Corning black low volume, low binding, 384-well plates at a final volume of 10 μL in the same manner as described above.

4.5. Protein X-ray Crystallography. *4.5.1. RORγt-LBD Expression and Purification (Used for Crystallography).* A pET15b expression vector was ordered from GenScript encoding for the RORγt LBD (residues 265−507) containing a C455H mutation (RORγtC455H) and a C-terminal His-tag. The plasmid was transformed by heat shock into BL21(DE3) *E. coli* cells. A single colony was used to start three precultures of 24 mL LB medium containing 100 μg/mL ampicillin. After overnight incubation at 37 °C, each preculture was transferred to 2 L of 2× YT medium supplied with 0.05% antifoam SE-15 (Sigma-Aldrich). These cultures were incubated until they reached an OD_{600} = 0.6. Protein expression was induced by adding 0.25 mM IPTG. The temperature was decreased to 15 °C, and protein expression proceeded overnight. The cells were collected by centrifugation at 10.000 RCF for 10 min at 4 °C. The resulting 30 g of cell pellet was dissolved in lysis buffer (20 mM Tris, 500 mM NaCl, 2 mM TCEP, 0.1% Tween20, 10% glycerol, 10 cOmplete Protease Inhibitor Cocktail tablets (Roche), and 25 U/mL Bezonase Nuclease (Millipore), adjusted to pH = 8.0). After cell lysis using an Emulsiflex-C3 homogenizer (Avestin), the cell lysate was cleared by centrifugation at 40.000 RCF for 40 min at 4 °C, and the supernatant was loaded on a 5 mL Ni-NTA Superflow cartridge (QIAGEN) pre-equilibrated with buffer A (20 mM Tris, 500 mM NaCl, 2 mM TCEP, 0.1% Tween20, and 10% glycerol). The column was washed with 10 CVs of buffer A supplied with 20 mM and sequentially with 10 CVs of Buffer A supplied with 50 mM imidazole. The protein was eluted from the resin using an eight column volumes elution buffer (buffer A supplied with 200 mM imidazole). The purified protein was then dialyzed overnight to buffer A containing 1.2 U of restriction-grade thrombin (Millipore) per milligram of purified protein to remove the His-tag. Next, the protein mixture was concentrated using an Amicon Ultra centrifugal filter with a 10-kDa cutoff (Millipore) and loaded on a Superdex 75 pg 16/60 size-exclusion column (GE Life Sciences) using 20 mM Tris, 100 mM NaCl, and 5 mM DTT (adjusted to pH = 8.0) as a running buffer. The flow-through was collected as 3 mL fractions which were analyzed using Q-ToF LC−MS. The fractions containing RORγtC455H were combined and concentrated to a final concentration of 11.1 mg/mL. The concentrated protein sample was then aliquoted, flash-frozen, and stored at −80 °C.

4.5.2. X-ray Crystallography. The RORγtC455H solution (11.1 mg/mL) was mixed with 2 equiv of **25** and incubated on ice for 1 h. Next, the sample was centrifuged at 20.000 RCF for 20 min at 4 °C to remove precipitated proteins. MRC-2 well crystallization plates (Hampton Research, sitting drop) were prepared using a Mosquito pipetting robot (TTP Labtech). Well-diffracting crystals were obtained by mixing 0.9 ul of protein solution with 0.3 μL of 1.6−2.0 M ammonium sulfate and 0.1 M Tris (pH = 8.5). The well was filled with 80 μL precipitant solution, and plates were placed at 20 °C. Crystals could be observed after 1 h of incubation and grew to their

DOI: 10.1021/acs.jmedchem.9b01372
J. Med. Chem. 2020, 63, 241−259

final size overnight. The crystals were cryoprotected by transferring the crystals briefly to a solution containing 1.2 M AmSO4, 0.1 M Tris (pH = 8.5), and 25% glycerol before being flash cooled in liquid N_2. Diffraction data were collected at 100 K at the P11 beamline of the PETRA III facility at DESY (Hamburg, Germany) and processed using the CCP4 suite (version 7.0.075).[46] DIALS was used to integrate and scale the data.[47] The data was phased with PHASER using 5C4O as a molecular replacement model and ligand restraints of **25** were generated with AceDRG.[48,49] Sequential model building and refinement were performed with COOT and REFMAC, respectively.[50,51] PyMOL (version 2.2.3, Schrödinger) was used to make the figures.[52] The structure of RORγtC455 in complex with **25** was deposited in the protein data bank (PDB) under code 6SAL.

4.6. Quantitative IL-17a mRNA RT-PCR Assay. EL4 cells (Sigma-Aldrich) were grown in DMEM (Gibco) with 10% FBS. At 24 h after the cells were seeded onto a 12-well plate, the cells were incubated with 10 μM compound (from 10 mM stock in DMSO) or DMSO for 24 h and activated with phorbol 12-myristate 13-acetate (PMA, 50 ng/mL; Sigma-Aldrich) and ionomycin (1 μg/mL; Sigma-Aldrich) for 5 h. The cells were then collected, and RNA was isolated using a RNeasy Mini Kit (Qiagen) and reverse transcribed using the iScript Advanced cDNA Synthesis Kit (Bio-Rad). Quantitative RT-PCR was performed to analyze mRNA levels of mouse IL-17a levels (in triplicate) using SYBR green technology (Bio-Rad) on a CFX Real-Time System (Bio-Rad). The following primer assays were purchased from Bio-Rad: IL-17a (qMmuCID0026592) and Gapdh (qMmuCED0027497). The level of IL-17a mRNA expression was normalized to that of Gapdh expression. The relative gene expression was calculated by the $2^{-\Delta\Delta Ct}$ (Livak) method using the DMSO control as calibrator. (Data recorded in triplicate; error shown is standard deviation from the mean; data are representative of >3 repeated experiments).

4.7. Absorption, Distribution, Metabolism, and Excretion Experiments. *4.7.1. Chemical Stability.* Chemical stability was determined by incubating test compounds at a final concentration of 2 μM in aqueous buffer at pH 7.4 for 1, 7, and 24 h, respectively. The percentage of remaining compound (% remain) in relation to the zero time point was calculated following LC−MS-based measurement of sample aliquots of each time point.

4.7.2. Kinetic Solubility. Aqueous solubility of compounds was determined by spectrophotometrical measurement of the kinetic solubility of a 500 μM compound solution in aqueous buffer pH 7.4 compared to a solution in the organic solvent acetonitrile after 90 min of vigorous shaking at room temperature.

4.7.3. PAMPA. Permeability through artificial membranes (PAMPA) was performed at an initial concentration of 500 μM of the compound in the donor compartment. After an incubation period of 20 h, absorption of the receiver wells was measured by spectrophotometry and permeation was calculated by normalization of the compound flux across a blank filter.

4.7.4. Microsomal Stability Phase I. Metabolic stability under oxidative conditions was measured in liver microsomes from different species by LC−MS-based measuring of depletion of compound at a concentration of 3 μM over time up to 50 min at 37 °C. On the basis of compound half-life $t_{1/2}$, in vitro intrinsic clearance CL_{int} was calculated. $CL_{int} = \frac{V \times 0.693}{t_{1/2} \times mg}$

4.7.5. Microsomal Stability Phase II. Metabolic stability under conjugative conditions was measured in the glucuronidation assay by LC−MS-based determination of % remaining of selected compounds at a concentration of 5 μM in incubations with liver microsomes supplemented with UDPGA for 1 h at 37 °C.

4.7.6. Plasma Stability. Plasma stability was measured by LC−MS-based determination of % remaining of selected compounds at a concentration of 5 μM after incubation in 100% plasma obtained from different species for 1 h at 37 °C.

4.7.7. Plasma Protein Binding. Assessment of plasma protein binding was measured by equilibrium dialysis by incubating plasma with the compound of interest at a concentration of 5 μM for 6 h at 37 °C followed by LC−MS-based determination of final compound concentrations.

■ ASSOCIATED CONTENT

Supporting Information

The Supporting Information is available free of charge at https://pubs.acs.org/doi/10.1021/acs.jmedchem.9b01372.

S1.0. In silico experiments: phase pharmacophore screen scores (Table S1 and S2), Chem-T C-5 virtual library SMILES strings (Table S3), manually generated C-5 virtual library (Figure S1), and glide docking scores (Tables S4 and S5); S2.0. Chemistry Supporting Information and Spectra: (S2.1) Regiochemical assignment of **30a**, (S2.2) synthesis of **5** (Glenmark) and (S2.3) NMR spectra and LC-UV traces for assayed compounds; and S3.0. Crystallography: data collection and refinement statistics (molecular replacement) of **25** (Table S6), two-dimensional protein−ligand interaction plot for **25** (Figure S2), and overlay of crystal structure and docking pose for **25** (Figure S3) (PDF)

Recommended compound characterization checklist (XLS)

Molecular formula strings (CSV)

Molecular formula strings (XLSX)

Accession Codes

Coordinates and structure factors for the RORγt bound to compound **25** have been deposited in the Protein Data Bank under accession code 6SAL. Authors will release the atomic coordinates and experimental data upon article publication.

■ AUTHOR INFORMATION

Corresponding Author

*E-mail: l.brunsveld@tue.nl.

ORCID

Femke A. Meijer: 0000-0003-4412-9968

Christian Ottmann: 0000-0001-7315-0315

Luc Brunsveld: 0000-0001-5675-511X

Author Contributions

ξF.A.M. and R.G.D. contributed equally to this work. The manuscript was written through contributions of all authors. R.G.D. and S.L. performed in silico work; R.G.D., F.A.M., G.M.V., and A.A.A.V. performed synthesis and biochemical studies; F.A.M. performed RT-PCR experiments; R.M.J.M.V. performed protein expression and crystallization studies; R.G.D., F.A.M., R.M.J.M.V., S.L., M.S., C.O., L.G.M., and L.B. designed the studies. All authors have given approval to the final version of the manuscript.

Funding

This work was supported by The Netherlands Organization for Scientific Research through Gravity program 024.001.035, VICI grant 016.150.366, ECHO grant 711.018.003, and the European Union through a MSCA Individual Fellowship (R.G.D., H2020-MSCA-IEF-2016, grant no. 705188).

Notes

The authors declare no competing financial interest.

■ ACKNOWLEDGMENTS

We thank Rowin J.P.M. de Visser for synthesis of the AlexaFluor647-labelled MRL-871 probe, Guido J.M. Oerlemans and Maxime C.M. van den Oetelaar for synthesis optimization, Iris A. Leijten-van de Gevel for expression of the

DOI: 10.1021/acs.jmedchem.9b01372
J. Med. Chem. 2020, 63, 241−259

RORγt protein (used for TR-FRET assays), and Joost L.J. van Dongen for performing HRMS measurements. We also thank the Lead Discovery Center in Dortmund (Matthias Baumann, Jan Eickhoff, and Bert Klebl) for performing ADME measurements. Finally, we thank the DLS-CCP4 Data Collection and Structure Solution Workshop 2017 at Diamond Light Source (Oxfordshire, UK).

■ ABBREVIATIONS USED

AR, androgen receptor; DME, 1,2-dimethoxyethane; DMF, dimethylformamide; DMP, Dess-Martin periodinane; DPPA, diphosphoryl azide; H12, helix 12; IPTG, isopropyl-*b*-d-thiogalactoside; mAb, monoclonal antibody; NBS, *N*-bromosuccinimide; NCS, *N*-chlorosuccinimide; NR, nuclear receptor; Q-tof, quadrupole time-of-flight; RORγt, retinoic acid receptor-related orphan receptor γ t; RT-PCR, real time PCR; TFA, trifluoroacetic acid; Th17, T helper 17; THF, tetrahydrofuran; TR-FRET, time-resolved FRET

■ REFERENCES

(1) Wang, J.; Zou, J. X.; Xue, X.; Cai, D.; Zhang, Y.; Duan, Z.; Xiang, Q.; Yang, J. C.; Louie, M. C.; Borowsky, A. D.; Gao, A.; Evans, C. P.; Lam, K. S.; Xu, J.; Kung, H.-J.; Evans, R. M.; Xu, Yong; Chen, H.-W. ROR-γ drives androgen receptor expression and represents a therapeutic target in castration-resistant prostate cancer. *Nat. Med.* **2016**, *22*, 488−496.

(2) Zhang, Y.; Wu, X.; Xue, X.; Li, C.; Wang, J.; Wang, R.; Zhang, C.; Wang, C.; Shi, Y.; Zou, L.; Li, Q.; Huang, Z.; Hao, X.; Loomes, K.; Wu, D.; Chen, H.-W.; Xu, J.; Xu, Y. Discovery and characterization of XY101, a potent, selective, and orally bioavailable RORγ inverse agonist for treatment of castration-resistant prostate cancer. *J. Med. Chem.* **2019**, *62*, 4716−4730.

(3) Ivanov, I. I.; McKenzie, B. S.; Zhou, L.; Tadokoro, C. E.; Lepelley, A.; Lafaille, J. J.; Cua, D. J.; Littman, D. R. The orphan nuclear receptor RORγt directs the differentiation program of proinflammatory IL-17+ T helper cells. *Cell* **2006**, *126*, 1121−1133.

(4) Manel, N.; Unutmaz, D.; Littman, D. R. The differentiation of human TH-17 cells requires transforming growth factor-*β* and induction of the nuclear receptor RORγt. *Nat. Immunol.* **2008**, *9*, 641−649.

(5) Yang, X. O.; Pappu, B. P.; Nurieva, R.; Akimzhanov, A.; Kang, H. S.; Chung, Y.; Ma, L.; Shah, B.; Panopoulos, A. D.; Schluns, K. S.; Watowich, S. S.; Tian, Q.; Jetten, A. M.; Dong, C. T helper 17 lineage differentiation is programmed by orphan nuclear receptors RORα and RORγ. *Immunity* **2008**, *28*, 29−39.

(6) Miossec, P.; Kolls, J. K. Targeting IL-17 and TH17 cells in chronic inflammation. *Nat. Rev. Drug Discovery* **2012**, *11*, 763−776.

(7) Burkett, P. R.; Kuchroo, V. K. IL-17 blockade in psoriasis. *Cell* **2016**, *167*, 1669.

(8) Lock, C.; Hermans, G.; Pedotti, R.; Brendolan, A.; Schadt, E.; Garren, H.; Langer-Gould, A.; Strober, S.; Cannella, B.; Allard, J.; Klonowski, P.; Austin, A.; Lad, N.; Kaminski, N.; Galli, S. J.; Oksenberg, J. R.; Raine, C. S.; Heller, R.; Steinman, L. Gene-microarray analysis of multiple sclerosis lesions yields new targets validated in autoimmune encephalomyelitis. *Nat. Med.* **2002**, *8*, 500−508.

(9) Duerr, R. H.; Taylor, K. D.; Brant, S. R.; Rioux, J. D.; Silverberg, M. S.; Daly, M. J.; Steinhart, A. H.; Abraham, C.; Regueiro, M.; Griffiths, A.; Dassopoulos, T.; Bitton, A.; Yang, H.; Targan, S.; Datta, L. W.; Kistner, E. O.; Schumm, L. P.; Lee, A. T.; Gregersen, P. K.; Barmada, M. M.; Rotter, J. I.; Nicolae, D. L.; Cho, J. H. A genome-wide association study identifies IL23R as an inflammatory bowel disease gene. *Science* **2006**, *314*, 1461−3.

(10) Hueber, W.; Patel, D. D.; Dryja, T.; Wright, A. M.; Koroleva, I.; Bruin, G.; Antoni, C.; Draelos, Z.; Gold, M. H.; Psoriasis Study Group; Durez, P.; Tak, P. P.; Gomez-Reino, J. J.; Rheumatoid Arthritis Study Group; Foster, C. S.; Kim, R. Y.; Samson, C. M.; Falk, N. S.; Chu, D. S.; Callanan, D.; Nguyen, Q. D.; Uveitis Study Group; Rose, K.; Haider, A.; Di Padova, F. Effects of AIN457, a fully human antibody to interleukin-17A, on psoriasis, rheumatoid arthritis, and uveitis. *Sci. Transl. Med.* **2010**, *2*, 52ra72.

(11) Attia, A.; Abushouk, A. I.; Ahmed, H.; Gadelkarim, M.; Elgebaly, A.; Hassan, Z.; Abdel-Daim, M. M.; Negida, A. Safety and efficacy of brodalumab for moderate-to-severe plaque psoriasis: A systematic review and meta-analysis. *Clin. Drug Invest.* **2017**, *37*, 439−451.

(12) Mease, P. J.; van der Heijde, D.; Ritchlin, C. T.; Okada, M.; Cuchacovich, R. S.; Shuler, C. L.; Lin, C. Y.; Braun, D. K.; Lee, C. H.; Gladman, D. D.; SPIRIT-P1 Study Group. Ixekizumab, an interleukin-17A specific monoclonal antibody, for the treatment of biologic-naive patients with active psoriatic arthritis: results from the 24-week randomised, double-blind, placebo-controlled and active (adalimumab)-controlled period of the phase III trial SPIRIT-P1. *Ann. Rheum. Dis.* **2017**, *76*, 79−87.

(13) Fauber, B. P.; Magnuson, S. Modulators of the nuclear receptor retinoic acid receptor-related orphan receptor-γ (RORγ or RORc). *J. Med. Chem.* **2014**, *57*, 5871−92.

(14) Bronner, S. M.; Zbieg, J. R.; Crawford, J. J. RORγ antagonists and inverse agonists: a patent review. *Expert Opin. Ther. Pat.* **2017**, *27*, 101−112.

(15) Pandya, V. B.; Kumar, S.; Sachchidanand; Sharma, R.; Desai, R. C. Combating autoimmune diseases with retinoic acid receptor-related orphan receptor-γ (RORγ or RORc) inhibitors: hits and misses. *J. Med. Chem.* **2018**, *61*, 10976−10995.

(16) Tanis, V. M.; Venkatesan, H.; Cummings, M. D.; Albers, M.; Kent Barbay, J.; Herman, K.; Kummer, D. A.; Milligan, C.; Nelen, M. I.; Nishimura, R.; Schlueter, T.; Scott, B.; Spurlino, J.; Wolin, R.; Woods, C.; Xue, X.; Edwards, J. P.; Fourie, A. M.; Leonard, K. 3-Substituted quinolines as RORγt inverse agonists. *Bioorg. Med. Chem. Lett.* **2019**, *29*, 1463−1470.

(17) Imura, C.; Ueyama, A.; Sasaki, Y.; Shimizu, M.; Furue, Y.; Tai, N.; Tsujii, K.; Katayama, K.; Okuno, T.; Shichijo, M.; Yasui, K.; Yamamoto, M. A novel RORγt inhibitor is a potential therapeutic agent for the topical treatment of psoriasis with low risk of thymic aberrations. *J. Dermatol. Sci.* **2019**, *93*, 176−185.

(18) Tian, J.; Sun, N.; Yu, M.; Gu, X.; Xie, Q.; Shao, L.; Liu, J.; Liu, L.; Wang, Y. Discovery of *N*-indanyl benzamides as potent RORγt inverse agonists. *Eur. J. Med. Chem.* **2019**, *167*, 37−48.

(19) Kotoku, M.; Maeba, T.; Fujioka, S.; Yokota, M.; Seki, N.; Ito, K.; Suwa, Y.; Ikenogami, T.; Hirata, K.; Hase, Y.; Katsuda, Y.; Miyagawa, N.; Arita, K.; Asahina, K.; Noguchi, M.; Nomura, A.; Doi, S.; Adachi, T.; Crowe, P.; Tao, H.; Thacher, S.; Hashimoto, H.; Suzuki, T.; Shiozaki, M. Discovery of second generation RORγ inhibitors composed of an azole scaffold. *J. Med. Chem.* **2019**, *62*, 2837−2842.

(20) Duan, J. J.; Lu, Z.; Jiang, B.; Stachura, S.; Weigelt, C. A.; Sack, J. S.; Khan, J.; Ruzanov, M.; Galella, M. A.; Wu, D. R.; Yarde, M.; Shen, D. R.; Shuster, D. J.; Borowski, V.; Xie, J. H.; Zhang, L.; Vanteru, S.; Gupta, A. K.; Mathur, A.; Zhao, Q.; Foster, W.; Salter-Cid, L. M.; Carter, P. H.; Dhar, T. G. M. Structure-based discovery of phenyl (3-phenylpyrrolidin-3-yl)sulfones as selective, orally active RORγt inverse agonists. *ACS Med. Chem. Lett.* **2019**, *10*, 367−373.

(21) Gronemeyer, H.; Gustafsson, J.-Å.; Laudet, V. Principles for modulation of the nuclear receptor superfamily. *Nat. Rev. Drug Discovery* **2004**, *3*, 950−964.

(22) Li, X.; Anderson, M.; Collin, D.; Muegge, I.; Wan, J.; Brennan, D.; Kugler, S.; Terenzio, D.; Kennedy, C.; Lin, S.; Labadia, M. E.; Cook, B.; Hughes, R.; Farrow, N. A. Structural studies unravel the active conformation of apo RORγt nuclear receptor and a common inverse agonism of two diverse classes of RORγt inhibitors. *J. Biol. Chem.* **2017**, *292*, 11618−11630.

(23) Harris, J. M.; Lau, P.; Chen, S. L.; Muscat, G. E. O. Characterization of the retinoid orphan-related receptor-alpha coactivator binding interface: a structural basis for ligand-independent transcription. *Mol. Endocrinol.* **2002**, *16*, 998−1012.

DOI: 10.1021/acs.jmedchem.9b01372
J. Med. Chem. 2020, 63, 241−259

(24) Hu, X.; Wang, Y.; Hao, L. Y.; Liu, X.; Lesch, C. A.; Sanchez, B. M.; Wendling, J. M.; Morgan, R. W.; Aicher, T. D.; Carter, L. L.; Toogood, P. L.; Glick, G. D. Sterol metabolism controls TH17 differentiation by generating endogenous RORγ agonists. *Nat. Chem. Biol.* **2015**, *11*, 141−147.
(25) Huh, J. R.; Leung, M. W.; Huang, P.; Ryan, D. A.; Krout, M. R.; Malapaka, R. R.; Chow, J.; Manel, N.; Ciofani, M.; Kim, S. V.; Cuesta, A.; Santori, F. R.; Lafaille, J. J.; Xu, H. E.; Gin, D. Y.; Rastinejad, F.; Littman, D. R. Digoxin and its derivatives suppress TH17 cell differentiation by antagonizing RORγt activity. *Nature* **2011**, *472*, 486−490.
(26) Kumar, N.; Solt, L. A.; Conkright, J. J.; Wang, Y.; Istrate, M. A.; Busby, S. A.; Garcia-Ordonez, R. D.; Burris, T. P.; Griffin, P. R. The benzenesulfoamide T0901317 [N-(2,2,2-trifluoroethyl)-N-[4-[2,2,2-trifluoro-1-hydroxy-1-(trifluoromethyl)ethyl]phenyl]-benzenesulfonamide] is a novel retinoic acid receptor-related orphan receptor-alpha/gamma inverse agonist. *Mol. Pharmacol.* **2010**, *77*, 228−236.
(27) Overington, J. P.; Al-Lazikani, B.; Hopkins, A. L. How many drug targets are there? *Nat. Rev. Drug Discovery* **2006**, *5*, 993−996.
(28) Meijer, F. A.; Leijten-van de Gevel, I. A.; de Vries, R. M. J. M.; Brunsveld, L. Allosteric small molecule modulators of nuclear receptors. *Mol. Cell. Endocrinol.* **2019**, *485*, 20−34.
(29) Tice, C. M.; Zheng, Y.-J. Non-canonical modulators of nuclear receptors. *Bioorg. Med. Chem. Lett.* **2016**, *26*, 4157−4164.
(30) Moore, T. W.; Mayne, C. G.; Katzenellenbogen, J. Not picking pockets: nuclear receptor alternate-site modulators (NRAMs). *Mol. Endocrinol.* **2010**, *24*, 683−95.
(31) Scheepstra, M.; Leysen, S.; van Almen, G. C.; Miller, J. R.; Piesvaux, J.; Kutilek, V.; van Eenennaam, H.; Zhang, H.; Barr, K.; Nagpal, S.; Soisson, S. M.; Kornienko, M.; Wiley, K.; Elsen, N.; Sharma, S.; Correll, C. C.; Trotter, B. W.; van der Stelt, M.; Oubrie, A.; Ottmann, C.; Parthasarathy, G.; Brunsveld, L. Identification of an allosteric binding site for RORγt inhibition. *Nat. Commun.* **2015**, *6*, 8833.
(32) Ouvry, G.; Bouix-Peter, C.; Ciesielski, F.; Chantalat, L.; Christin, O.; Comino, C.; Duvert, D.; Feret, C.; Harris, C. S.; Lamy, L.; Luzy, A. P.; Musicki, B.; Orfila, D.; Pascau, J.; Parnet, V.; Perrin, A.; Pierre, R.; Polge, G.; Raffin, C.; Rival, Y.; Taquet, N.; Thoreau, E.; Hennequin, L. F. Discovery of phenoxyindazoles and phenylthioindazoles as RORγ inverse agonists. *Bioorg. Med. Chem. Lett.* **2016**, *26*, 5802−5808.
(33) Guo, Y.; MacIsaac, K. D.; Chen, Y.; Miller, R. J.; Jain, R.; Joyce-Shaikh, B.; Ferguson, H.; Wang, I. M.; Cristescu, R.; Mudgett, J.; Engstrom, L.; Piers, K. J.; Baltus, G. A.; Barr, K.; Zhang, H.; Mehmet, H.; Hegde, L. G.; Hu, X.; Carter, L. L.; Aicher, T. D.; Glick, G.; Zaller, D.; Hawwari, A.; Correll, C. C.; Jones, D. C.; Cua, D. J. Inhibition of RORγT skews TCRα gene rearrangement and limits T cell repertoire diversity. *Cell Rep.* **2016**, *17*, 3206−3218.
(34) Zhong, C.; Zhu, J. Small-molecule RORγt antagonists: one stone kills two birds. *Trends Immunol.* **2017**, *38*, 229−231.
(35) Gege, C. Retinoid-related orphan receptor γ t modulators: comparison of Glenmark's me-too patent application (WO2015008234) with the originator application from Merck Sharp and Dohme (WO2012106995). *Expert Opin. Ther. Pat.* **2015**, *25*, 1215−1221.
(36) Dixon, S. L.; Smondyrev, A. M.; Knoll, E. H.; Rao, S. N.; Shaw, D. E.; Friesner, R. A. PHASE: A new engine for pharmacophore perception, 3D QSAR model development, and 3D database screening: 1. Methodology and preliminary results. *J. Comput.-Aided Mol. Des.* **2006**, *20*, 647−671.
(37) Dixon, S. L.; Smondyrev, A. M.; Rao, S. N. PHASE: A novel approach to pharmacophore modeling and 3D database searching. *Chem. Biol. Drug Des.* **2006**, *67*, 370−372.
(38) Asinex Corp. Gold and platinum collections, release: 1994−2004, update: 2016−10, www.asinex.com/libraries-html/libraries_gold_platinum-html.
(39) Kalin, J. H.; Zhang, H.; Gaudrel-Grosay, S.; Vistoli, G.; Kozikowski, A. P. Chiral mercaptoacetamides display enantioselective inhibition of histone deacetylase 6 and exhibit neuroprotection in cortical neuron models of oxidative stress. *ChemMedChem* **2012**, *7*, 425−39.
(40) Friesner, R. A.; Banks, J. L.; Murphy, R. B.; Halgren, T. A.; Klicic, J. J.; Mainz, D. T.; Repasky, M. P.; Knoll, E. H.; Shelley, M.; Perry, J. K.; Shaw, D. E.; Francis, P.; Shenkin, P. S. Glide: A new approach for rapid, accurate docking and scoring. 1. method and assessment of docking accuracy. *J. Med. Chem.* **2004**, *47*, 1739−1749.
(41) Halgren, T. A.; Murphy, R. B.; Friesner, R. A.; Beard, H. S.; Frye, L. L.; Pollard, W. T.; Banks, J. L. Glide: A new approach for rapid, accurate docking and scoring. 2. enrichment factors in database screening. *J. Med. Chem.* **2004**, *47*, 1750−1759.
(42) Abreu, R. M. V.; Froufe, H. J. C.; Daniel, P. O. M.; Queiroz, M. J. R. P.; Ferreira, I. C. F. R. ChemT, an open-source software for building template-based chemical libraries. *SAR QSAR Environ. Res.* **2011**, *22*, 603−610.
(43) Leroy, J. Preparation of 3-bromopropiolic esters: methyl and tert-butyl 3-bromopropiolates. *Org. Synth.* **1997**, *74*, 212.
(44) Oakdale, J. S.; Sit, R. K.; Fokin, V. V. Ruthenium-catalyzed cycloadditions of 1-haloalkynes with nitrile oxides and organic azides: synthesis of 4-haloisoxazoles and 5-halotriazoles. *Chem. - Eur. J.* **2014**, *20*, 11101−11110.
(45) Buckman, D. O.; Nicholas, J. B.; Emayan, K.; Seiwert, S. D.; Yuan, S. Lysophosphatidic acid receptor antagonists. International patent WO/2014/113485, 2014.
(46) Potterton, L.; Agirre, J.; Ballard, C.; Cowtan, K.; Dodson, E.; Evans, P. R.; Jenkins, H. T.; Keegan, R.; Krissinel, E.; Stevenson, K.; Lebedev, A.; McNicholas, S. J.; Nicholls, R. A.; Noble, M.; Pannu, N. S.; Roth, C.; Sheldrick, G.; Skubak, P.; Turkenburg, J.; Uski, V.; von Delft, F.; Waterman, D.; Wilson, K.; Winn, M.; Wojdyr, M. CCP412: the new graphical user interface to the CCP4 program suite. *Acta Crystallogr. D. Struct. Biol.* **2018**, *74*, 68−84.
(47) Clabbers, M. T. B.; Gruene, T.; Parkhurst, J. M.; Abrahams, J. P.; Waterman, D. G. Electron diffraction data processing with DIALS. *Acta Crystallogr. D. Struct. Biol.* **2018**, *74*, 506−518.
(48) McCoy, A. J. Solving structures of protein complexes by molecular replacement with Phaser. *Acta Crystallogr., Sect. D: Biol. Crystallogr.* **2007**, *63*, 32−41.
(49) Long, F.; Nicholls, R. A.; Emsley, P.; Grazulis, S.; Merkys, A.; Vaitkus, A.; Murshudov, G. N. *AceDRG:* a stereochemical description generator for ligands. *Acta Crystallogr. D. Struct. Biol.* **2017**, *73*, 112−122.
(50) Emsley, P.; Lohkamp, B.; Scott, W. G.; Cowtan, K. Features and development of Coot. *Acta Crystallogr., Sect. D: Biol. Crystallogr.* **2010**, *66*, 486−501.
(51) Murshudov, G. N.; Skubák, P.; Lebedev, A. A.; Pannu, N. S.; Steiner, R. A.; Nicholls, R. A.; Winn, M. D.; Long, F.; Vagin, A. A. *REFMAC5* for the refinement of macromolecular crystal structures. *Acta Crystallogr., Sect. D: Biol. Crystallogr.* **2011**, *67*, 355−367.
(52) *The PyMOL Molecular Graphics System, version 2.2.3*; Schrödinger, LLC, 2000.

DOI: 10.1021/acs.jmedchem.9b01372
J. Med. Chem. 2020, 63, 241−259